

Slow spatial migration can help eradicate cooperative antimicrobial resistance in time-varying environments

Lluís Hernández-Navarro^{1,*,\dagger}, Kenneth Distefano^{2,*},
Uwe C. Täuber^{2,3}, and Mauro Mobilia^{1,\#}

¹Department of Applied Mathematics, School of Mathematics,
University of Leeds, Leeds LS2 9JT, U.K.

²Department of Physics & Center for Soft Matter and Biological Physics, MC 0435,
Robeson Hall, 850 West Campus Drive, Virginia Tech, Blacksburg, VA 24061, USA

³Faculty of Health Sciences, Virginia Tech, Blacksburg, VA 24061, USA

*These authors contributed equally to this work

^{\dagger}L.Hernandez-Navarro@leeds.ac.uk, ^{\#}M.Mobilia@leeds.ac.uk

December 30, 2024

Abstract

Antimicrobial resistance (AMR) is a global threat and combating its spread is of paramount importance. AMR often results from a cooperative behaviour with shared protection against drugs. Microbial communities generally evolve in volatile environments and spatial structures. Migration, fluctuations, and environmental variability thus have significant impacts on AMR, whose maintenance in static environments is generally promoted by migration. Here, we demonstrate that this picture changes dramatically in *time-fluctuating* spatially structured environments. To this end, we consider a two-dimensional metapopulation model consisting of demes in which drug-resistant and sensitive cells evolve in a time-changing environment in the presence of a toxin against which protection can be shared. Cells migrate between neighbouring demes and hence connect them. When the environment varies neither too quickly nor too slowly, the dynamics is characterised by bottlenecks causing fluctuation-driven local extinctions, a mechanism countered by migration that rescues AMR. Through simulations and mathematical analysis, we investigate how migration and environmental variability influence the probability of resistance eradication. We determine the near-optimal conditions for the fluctuation-driven AMR eradication, and show that slow but non-zero migration speeds up the clearance of resistance and can enhance its eradication probability. We discuss our study's impact on laboratory-controlled experiments.

1 Main

Microbial communities generally live in volatile, time-varying environments embedded in complex spatial structures connected through cellular migration, e.g., in soil [1], seabed [2], on wet surfaces [3], in plants [4], animals [5], and humans [6, 7]. How the environment helps shape microbial populations and species diversity [8, 9, 10, 11] is a subject of intense research [11, 12, 13, 14, 15, 16, 17, 18, 19, 20, 21, 22]. Moreover, environmental variability and microbiome-environment interactions greatly influence the evolution of microbial communities, with a growing interest in their eco-evolutionary dynamics [6, 10, 22, 23, 24, 25, 26, 27, 28]. Despite significant recent progress [13, 14, 21, 22], a general understanding of the joint influence of spatial structure and environmental variability on the evolution of microbial populations remains an open question that is notably relevant to the spread

of antimicrobial resistance (AMR) [29, 30, 31]. The evolution of AMR is of paramount societal importance, and is influenced by spatial structure, environmental changes and fluctuations. The latter are often associated with population bottlenecks [10], when the community size is drastically reduced, e.g., due to the effects of a drug [32, 33] or to other causes [34, 35]. The size and composition of microbial populations are often interdependent, leading to coupled environmental and demographic fluctuations [23, 26, 27, 28, 36, 37, 38, 39, 40, 41]. These are particularly relevant when antibiotics cause bottlenecks following which surviving cells may replicate and AMR can spread [33]. Recent studies have investigated the impact of space on the emergence and spread of non-cooperative AMR mutants [11, 15], even in the presence of environmental bottlenecks [20, 22]. However, AMR often results from cooperative behaviour with resistant microbes inactivating toxins and sharing their protection with drug-sensitive bacteria [21, 35, 42]. Recent research on cooperative AMR has mostly focused on microbiome-environment interactions [14, 21], without considering external environmental changes.

Here, inspired by β -lactamase cooperative AMR [35, 42, 43], we study how the migration of cells shapes the evolution of AMR in a spatially structured microbial population subject to environmental variability causing bottlenecks and fluctuations. To this end, we investigate the *in silico* evolution of cooperative antimicrobial resistance in a two-dimensional (2D) metapopulation consisting of cells that are either sensitive (S) or resistant (R) to a drug. In this explicit spatial model, the microbial community consists of a grid of linear size L , containing $L \times L$ demes whose well-mixed sub-populations are connected by cell migration (at a rate m), and is subject to a constant antimicrobial input and a time-fluctuating environment. We model environmental variability by letting the carrying capacity of each deme, $K \in \{K_-, K_+\}$, randomly switch back and forth between $K = K_+$, when the environment is mild, and $K = K_- < K_+$ under harsh conditions, across the entire metapopulation at frequencies ν_+ and ν_- (Fig. 1a). Whenever the number N_R of R cells in a deme exceeds a cooperative threshold N_{th} , the protection against the drug becomes a public good and is shared with all the N_S sensitive bacteria in that deme, whereas the number of cells in each deme fluctuates with K (Fig. 1b). In this setting, we investigate how cell migration and environmental fluctuations influence the evolution of antimicrobial resistance, and under which circumstances all resistant cells can be eradicated from the entire metapopulation.

2 Results

2.1 Bottlenecks can cause resistance fluctuation-driven eradication in isolated demes

It is useful to first address the evolution of R and S cells in a single isolated deme (Fig. 1a). When the environment varies either very quickly or slowly compared to the intra-deme dynamics, the eradication of R cannot be observed as resistant cells generally survive for extended periods [26] (Methods and Supplementary Section S2 of the Supplementary Information, at the end of this manuscript). Here, we focus on environments varying at an intermediate switching rate, neither too fast nor too slow, allowing the size of a deme to track the switching carrying capacity (Extended Data Fig. 8a and Methods, Supplementary Fig. S1), and assume $N_{\text{th}} < K_- < K_+$. In this biologically relevant regime [44, 45], when the environment switches from mild to harsh and the carrying capacity from K_+ to K_- , the population experiences bottlenecks, and demes contain generally more S bacteria than R cells (blue arrows in the sample paths of Fig. 1a (bottom), Supplementary Movies can be found at the OSF data repository osf.io/epb28, see Data availability section, with full description of the movies in the Supplementary Information Section S3). Henceforth, we quantify the bottleneck strength as K_+/K_- , which also serves as a measure of environmental variability. We have demonstrated that in intermediate-switching environments, in a well-mixed population subject to strong bottlenecks (large K_+/K_-), fluctuations cause the extinction of R cells when $K_+/K_- \gtrsim N_{\text{th}}$ on an average time $4/(\nu_+ + \nu_-)$ (Fig. 1a bottom, Methods) [26]. This phenomenon where resistance is cleared by the coupled effect of environmental and demographic fluctuations is called “fluctuation-driven eradication” (Methods). In this work, we investigate under which conditions this resistance eradication mechanism can hold in a two-dimensional metapopulation. This is an important and intriguing question since microbial communities generally evolve in spatial settings, and locally R -free demes can be recolonized by cells migrating from neighbouring sites (migration from cross to asterisk deme in Fig. 1b). Migration is thus

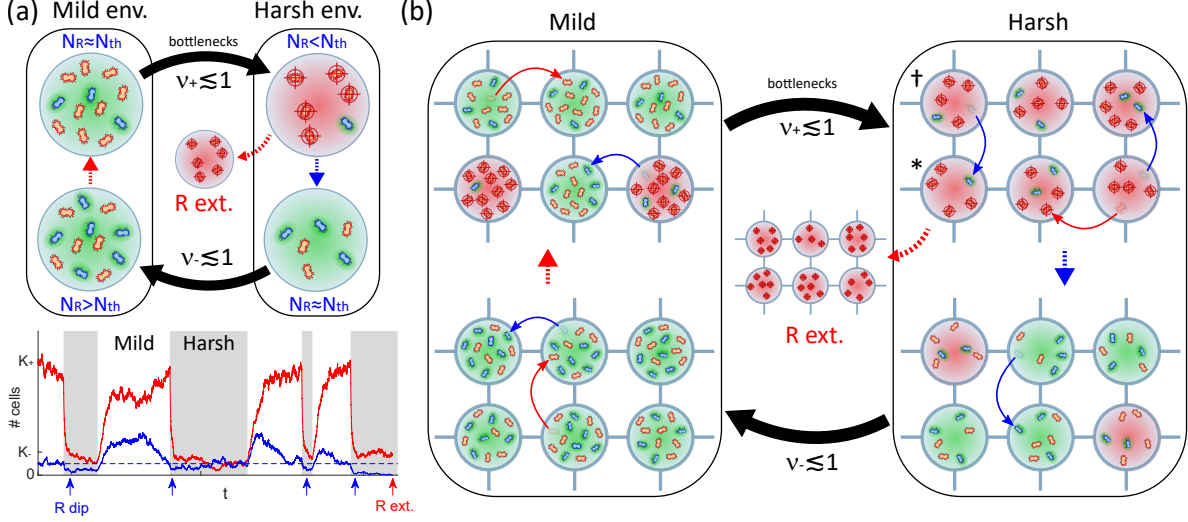


Figure 1: **Microbial community model.** (a) Eco-evolutionary dynamics in a single isolated deme ($m = 0$) subject to constant antimicrobial input and intermediate environmental switching, a regime where fluctuations can cause AMR eradication (Methods). **Top, schematic.** Illustrative evolution in an isolated deme with cooperation threshold $N_{th} = 3$, when the environment switches between mild ($K_+ = 12$) and harsh ($K_- = 6$) conditions at rates ν_+ and ν_- , with $\nu_{\pm} \lesssim 1$ (Supplementary Fig. S1 and Supplementary Section S3). Each resistant microbe (blue cells, R) produces a resistance enzyme that locally inactivates the drug (green shade) at a metabolic cost reducing their growth rate. When the number of R cells exceeds the threshold, $N_R \geq N_{th}$, the drug is inactivated in the entire deme and sensitive cells (red cells, S) benefit from the shared protection (public good) at no metabolic cost (green background shade, bottom left). This leads to an increase of the S fraction in the deme (upward dashed red arrow). When $N_R < N_{th}$, the drug is active (red background shade, top-right) and the spread of S cells is hampered (red cross hairs) while R cells are protected and thrive (dashed blue arrow). If $N_R > N_{th}$ in the mild environment (left black box), where the carrying capacity is $K = K_+$, the number of R cells decreases and evolves towards the cooperation threshold, $N_R \rightarrow N_{th}$, whereas the number N_S of sensitive microbes approaches $K_+ - N_{th}$ (upward dashed arrow). Similarly, if $N_R < N_{th}$ in the harsh environment (right box), where $K = K_-$, the number of R increases, with $N_R \rightarrow N_{th}$, while $N_S \rightarrow K_- - N_{th}$ (downward dashed arrow). To model environmental volatility, we assume that K suddenly switches back and forth between K_+ and K_- , driving the deme population size ($N = N_S + N_R$). In the intermediate switching regime, when $\nu_{\pm} \lesssim 1$, the population in the deme experiences bottlenecks whenever the environment changes from mild ($K = K_+$) to harsh ($K = K_-$). When $K_+/K_- \gtrsim N_{th}$ [26] (Methods), there is a chance that demographic fluctuations cause the extinction of R cells after each bottleneck (curved dashed red arrow). **Bottom, sample paths.** Stochastic realisations of the number of S (red curve) and R cells (blue solid curve) in a deme vs. time (Methods), with parameters $N_{th} = 40$ (blue dashed line), $K_+ = 400$, $K_- = 80$, $\nu_+ = 0.075$, and $\nu_- = 0.125$. White/grey background indicates mild/harsh environment. Population bottlenecks (interface between white and grey background) enforce transient dips of N_R (blue arrows) paving the way to fluctuation-driven R eradication (red arrow). (b) Eco-evolutionary dynamics in the 2D metapopulation; legend and parameters are as in (a). The population is structured as a two-dimensional grid of connected demes (with periodic boundary conditions), all with the same carrying capacity $K(t) \in \{K_-, K_+\}$. Each R and S cell can migrate onto a neighbouring deme with a rate m (curved red and blue arrows, Methods). Owing to local fluctuations, drug inactivation varies from one deme to another: it occurs in demes where $N_R \geq N_{th}$ (different green and red background shades). Following population bottlenecks, R can be locally extinct, e.g. in deme (*), but migration from a neighbouring site (\dagger) can rescue resistance (curved blue arrow between demes \dagger and *). Resistance is eradicated from the metapopulation when no R cells survive across the entire grid (curved dashed red arrow pointing to red-only metapopulation).

expected to generally favour the coexistence of R and S cells across the metapopulation (Extended Data Fig. 8d, Supplementary Fig. S2 and Supplementary Section S2), and more generally promotes bacterial diversity [46]. However, we show that fluctuation-driven eradication also occurs on the 2D grid and unveils an intriguing regime where migration even enhances this phenomenon of resistance clearance.

2.2 Critical migration rate and bottleneck strength to eradicate antimicrobial resistance

To study the eradication of resistance in the 2D metapopulation, we focus on the regime of intermediate environmental switching and moderate/slow migration, where $0 < m \lesssim 1$. This corresponds to each deme experiencing bottlenecks with a frequency of order $(\nu_+ + \nu_-)/4$, leading to local R eradication in a time scaling with $1/(\nu_+ + \nu_-)$ (Fig. 1a bottom and Methods), and single cells migrating between nearest-neighbour sites on a similar or slower time scale (Figs. 2 and 3). This results in demes being neither entirely isolated ($m = 0$), nor all fully connected (fast migration, $m \gg 1$), and spatial structure shaping the microbial dynamics. Since any R -free deme can be recolonised by resistant cells migrating in (Fig. 1b), it is not obvious whether eradication of resistance can arise in the spatial metapopulation. We find that environmental conditions causing strong bottlenecks, i.e. larger K_+/K_- values, increase the chances of clearing resistance across all demes (red/dark phase in Fig. 2a and Extended Data Fig. 7). This effect is countered by fast migration: when m is increased and many cells migrate between two consecutive bottlenecks, the fluctuation-driven eradication of R cells is severely suppressed (white/light phase in Figs. 2a and 4, and Extended Data Fig. 7). Remarkably, there is a trade-off between these contrasting effects, and we have determined the minimum bottleneck strength K_+/K_- and maximum migration rate m_c for which fluctuations can clear resistance across the whole metapopulation in a finite time (border between dark-red and light phases in Fig. 2a, see Fig. 2b-j). The critical migration rate m_c can be estimated by matching the number of R migration events between two successive bottlenecks with the number of new R -free demes in each bottleneck. In the intermediate switching regime, this argument yields (Methods)

$$m_c \simeq \frac{\nu_+ \nu_-}{2\nu N_{\text{th}} \left(\exp\left\{ \frac{N_{\text{th}} K_-}{K_+} \right\} - 1 \right)}, \quad (1)$$

where $\nu = (\nu_- + \nu_+)/2$ is the average switching rate. This analytical prediction approximately captures the border between the red/white phases and how m_c increases with K_+/K_- in a biologically relevant regime (green lines in Fig. 2a and Fig. 4a-e). The fluctuation-driven eradication of R across the 2D metapopulation hence requires intermediate environmental switching, strong enough bottlenecks, and slow to moderate migration, which can be summarised by (Fig. 2a; Fig. 4, Extended Data Fig. 7; Methods):

$$\nu \lesssim 1, \quad \frac{K_+}{K_-} \gtrsim N_{\text{th}} \quad \text{and} \quad m \lesssim m_c. \quad (2)$$

These conditions are valid when the bottleneck frequency is comparable to the rate of change of the deme composition (Methods). Furthermore, we have found that very strong bottlenecks, $K_+/K_- \gtrsim N_{\text{th}} L^2$, can eradicate R from all demes at once, regardless of the migration rate (Methods). Moreover, when there are fewer single cell migrations between two successive bottlenecks than demes in the metapopulation, migration is effectively irrelevant (equal red levels for $m \in [0, 10^{-3.5}]$ in Fig. 2a and for $m \in [0, 10^{-4.5}]$ in Fig. 4a-e; Methods).

2.3 Breaking it down: bottlenecks and fluctuations vs. spatial mixing

To understand the joint influence of bottlenecks and migration on R eradication, we analyse the typical time evolution of the metapopulation subject to intermediate switching and migration rates, with moderate bottleneck strength (Fig. 3, where $K_+/K_- = 25$, Supplementary Section S3 Movie 3). The microbial composition of a single deme fluctuates due to environmental switches and random birth-death events, until demographic fluctuations eventually lead to R eradication in the deme (Fig. 3a). This resistance clearance mechanism, driven by bottlenecks and fluctuations, occurs randomly across the 2D grid (scattered red sites in Fig. 3e). However, R cells can randomly migrate from neighbouring demes and recolonise resistant-free sites (Fig. 3b). Recolonisation can spread in space, favouring

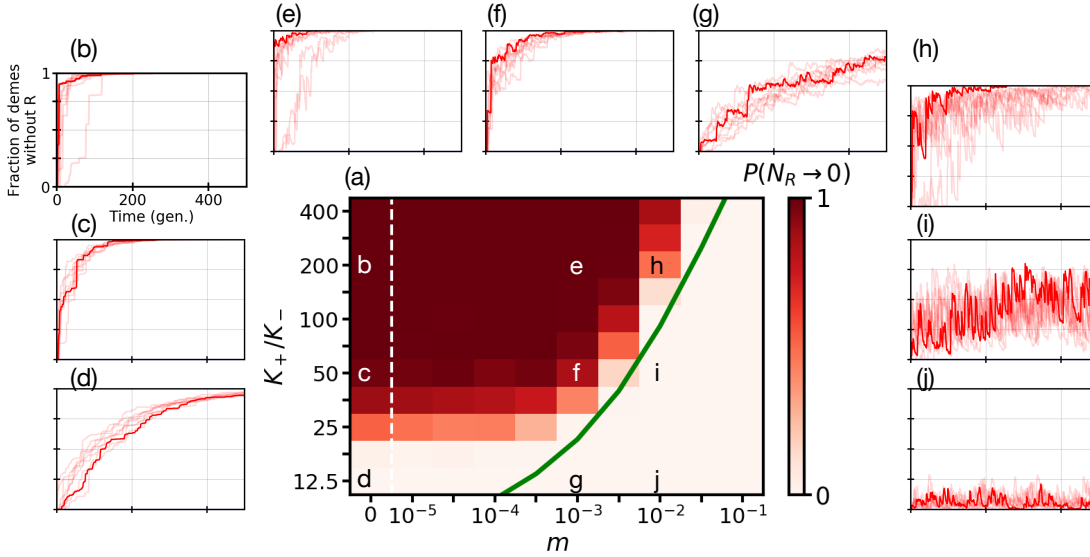


Figure 2: **The eradication mechanism of R cells depends on the bottleneck strength and migration rate.** The shared parameters in all panels are $\nu = 1$, $\delta = 0.75$, $L = 20$, $a = 0.25$, $s = 0.1$, $N_{\text{th}} = 40$, and $K_- = 80$ (Methods) with migration according to (7). Other parameters are as listed in Extended Data Table 1 (Methods). (a) Heatmap of the probability of total extinction of R (resistant) cells, $P(N_R \rightarrow 0)$, as a function of bottleneck strength, K_+/K_- , and migration rate m . Each $(m, K_+/K_-)$ value pair represents an ensemble average of 200 independent simulations, where we show the fraction of realisations resulting in complete extinction of R (resistant) microbes, given by $P(N_R \rightarrow 0)$, after running each realisation for 500 microbial generations (Methods). The colour bar ranges from light to dark red, where darkest red indicates that complete extinction of R was found in all 200 simulations, $P(N_R \rightarrow 0) = 1$. The green line is the theoretical prediction of Eq. (1) (Discussion and Methods) and the white dashed vertical line indicates an axis break separating $m = 0$ and $m = 10^{-5}$ (Methods). The black and white annotated letters point to the specific $(m, K_+/K_-)$ values used in the outer panels. (b-j) Typical example trajectories of the fraction of demes without R cells (fixation of sensitive cells) as a function of time (microbial generations) for several specific $(m, K_+/K_-)$ values as indicated in panel (a). One example trajectory out of ten is marked in bright red for visualization purposes.

microbial coexistence (pink clusters in Fig. 3e-f). Hence, the occurrence of bottlenecks increases the fraction of R -free demes across the grid (one spike for each bottleneck of Fig. 3d), whereas recolonisation reduces the fraction of S -only sites, leading to decays following bottleneck-induced spikes (Fig. 3d). Spikes are higher the stronger the bottlenecks, i.e. larger K_+/K_- , while the decreases steepen for faster migration, i.e. faster migration rates m (Fig. 2b-j and Methods). In the example of Fig. 3, the number of R -free demes steadily increases with the number of bottlenecks and, migration not being fast enough to rescue resistance in sufficient sites, R cells are eventually eradicated across the whole metapopulation (more red in Fig. 3g-h than in Fig. 3e-f; fraction of R -free demes approaches one in Fig. 3d; Supplementary Section S3 Movie 3).

2.4 Slow migration can speed up and enhance resistant cells' eradication

We have disentangled the trade-off between the population bottleneck strength K_+/K_- and the migration rate m . To further clarify the interplay between fluctuations and migration in the 2D metapopulation, we investigate how this trade-off depends on m and K_+/K_- over time, and how it changes for different values of the switching rate (Fig. 4 and Extended Data Fig. 7, Supplementary Fig. S3). Under the conditions (2), the overall resistance eradication probability increases in time (Fig. 4a-e): the R eradication mechanism overcomes microbial mixing, and the red phase expands in time until it reaches its border where $m \approx m_c$ (Eqs. (1) and (2); Methods). Remarkably, R cells in Fig. 4 are most likely to be eradicated from the metapopulation under slow but non-zero migration (red regions

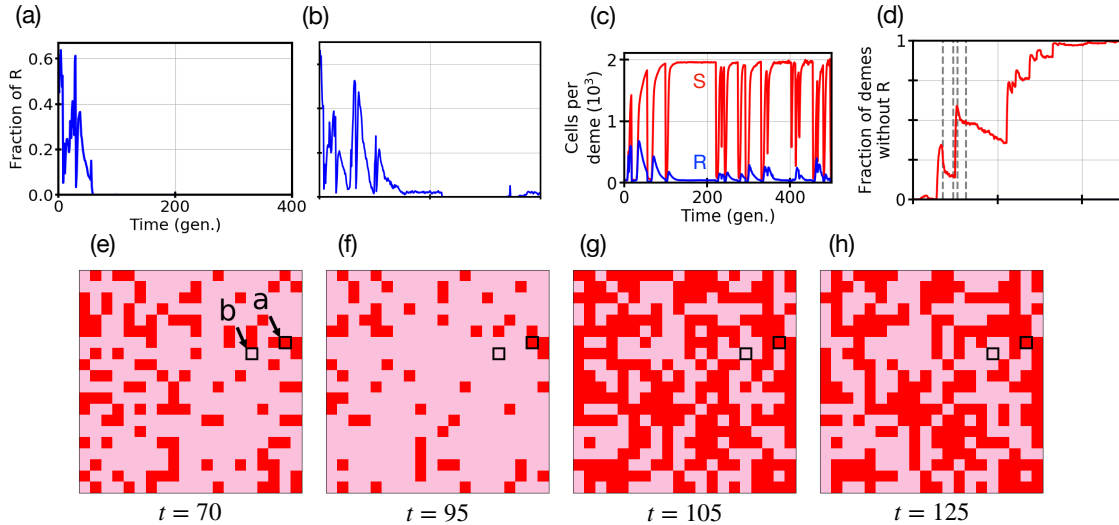


Figure 3: A closer look into individual demes: The effects of migration and intermediate environment switches on eradication of R cells. An example of the eco-evolutionary dynamics of a single metapopulation simulation with a mild environment carrying capacity $K_+ = 2000$, environmental switching rate $\nu = 0.1$, bias $\delta = 0.5$, and density-dependent migration according to (7) with migration rate $m = 0.001$ (Supplementary Section S3 Movie 3). Other parameters are as in Extended Data Table 1 (Methods). **(a-b)** Time evolution of the fraction of R (resistant) microbes, $N_R(\bar{u})/N(\bar{u})$, at two different demes where \bar{u} are the specific demes of interest; see highlighted demes in panels (e-h). The composition of the deme shown in panel (a) initially experiences coexistence and subsequent eradication of R cells due to environmental switches and demographic fluctuations. In panel (b), there is also coexistence and then eradication of R that is followed by recovery of R cells through recolonisation, as indicated by the series of blue spikes at long times (Discussion). **(c)** Average number of S and R cells in demes with both types of cells (pink pixels in panels (e-h)) versus time, obtained by sampling the make-up of all demes of the metapopulation that are not entirely populated by cells of only one type. In the regime of fluctuation-driven eradication, strain-coexisting demes consist of a majority of S cells ($N_{th} < K_- \ll K_+$) and subsequent bottlenecks cause sharp dips in the number of R and S per coexisting deme, following which demographic fluctuations can drive R cells to eradication. **(d)** Time evolution of the fraction of demes without R cells (red demes within panels (e-h)). From left to right, four dashed grey lines are shown at the specific times in which the snapshots are taken in panels (e-h). **(e-h)** Snapshots of the 20×20 metapopulation at four specific microbial generation times during the simulation, $t \in \{70, 95, 105, 125\}$. A red square is a deme experiencing eradication of R cells (only S cells are present), whereas a pink square is a deme displaying coexistence. The two demes of interest corresponding to panels (a-b) are indicated by a black border surrounding the deme. Panel (e) shows the metapopulation a few generations after an environmental bottleneck. From panels (e) to (f), there is an increase in pink demes due to migration of R cells causing S -only demes to become coexisting demes. Then, between $t = 95$ and $t = 105$, the metapopulation experiences a bottleneck that causes a burst of R -free demes (burst of red pixels at random locations in panel (g), spike in the number of eradicated R demes of panel (d)). Again, expanding pink clusters are shown in panel (h) due to migration of R cells after 20 generations. Supplementary Section S3 Movie 3 shows the full spatial metapopulation dynamics for these parameters.

in Fig. 4c-e at $m \sim 10^{-4} - 10^{-3}$ darker than at $m \sim 0 - 10^{-4.5}$; Supplementary Section S3 Movies 1-2). The probability of R eradication (S fixation) thus rapidly increases and plateaus near 1 for $m \sim 10^{-4} - 10^{-3}$ (Fig. 4f): for these migration rates, which are comparable to those realised in microfluidic experiments [47], the clearance of resistance is almost guaranteed. Furthermore, we have studied the R eradication probability as function of K_+/K_- and m for a range of slow, intermediate and fast switching rates ν , confirming that R eradication occurs chiefly for $0.1 \lesssim \nu \lesssim 1$ (Extended

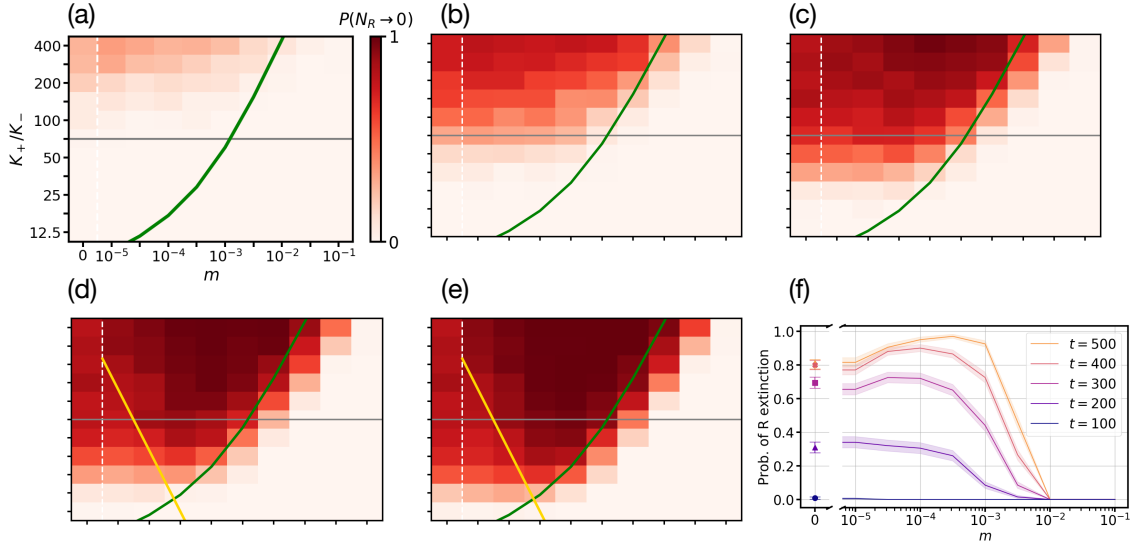


Figure 4: **Slow migration can speed up and enhance the eradication of R cells.** Time evolution of the heatmap showing the probability of R extinction $P(N_R \rightarrow 0)$ as a function of bottleneck strength, K_+/K_- , and migration rate m (implemented according to (7)) at (a) $t = 100$, (b) $t = 200$, (c) $t = 300$, (d) $t = 400$, and (e) $t = 500$ with environmental switching rate $\nu = 0.1$ and bias $\delta = 0.5$; other parameters are as in Extended Data Table 1 (Methods). As in Fig. 2a, each $(m, K_+/K_-)$ value pair is an ensemble of 200 independent metapopulation simulations and the $P(N_R \rightarrow 0)$ colour bar ranges from light to dark red indicating the fraction of simulations that have eradicated R cells at each snapshot in time. The green and dashed white lines represent the theoretical prediction of Eq. (1) and an eye-guiding axis break, respectively (as in Fig. 2a). The golden lines in panels (d-e) show $K_+/K_- = \frac{\nu}{mK_-}$, with $P(N_R \rightarrow 0) \approx 1$ in the (upper) region between the golden and green lines, according to Eq. (3) (Discussion). The grey horizontal lines in panels (a-e) indicate the example bottleneck strength of panel (f). (f) Probability of R extinction $P(N_R \rightarrow 0)$ as a function of migration rate m at bottleneck strength $K_+/K_- = 70.7$. Solid lines (full symbols at $m = 0$) indicate average across 200 realisations; shaded areas (error bars at $m = 0$) indicate binomial confidence interval computed via the Wald interval (Methods).

Data Fig. 7 and Supplementary Fig. S3).

These results demonstrate that not only does fluctuation-driven eradication of the resistant strain R arise in the 2D metapopulation under the conditions (2), but that slow migration ($0 < m < m_c$) actually *speeds up* the clearance of resistance and it *can even enhance* the probability of R eradication (Methods and Supplementary Section S3 Movie 2). When resistant cells randomly take over a deme during periods in the harsh environment, with the low carrying capacity $K = K_-$ (blue in Extended Data Fig. 6c,e, Supplementary Sections S2-S3 and Movie 1), the fluctuation-driven eradication mechanism does not work on this deme in isolation any more. However, slow migration rates allow sensitive cells to recolonise the deme and make it susceptible to R eradication (Methods and Extended Data Fig. 8, Supplementary Section S3 Movie 2).

3 Discussion

Microbial communities live in time-fluctuating environments endowed with spatial structure. Migration in space, environmental variability, and fluctuations thus affect the eco-evolutionary dynamics of bacterial populations [48]. They are particularly relevant to determine the likelihood that cells resistant to antimicrobial drugs survive AMR treatment or thrive in drug-polluted environments [10, 32, 33, 34, 35]. Understanding the joint influence of spatial structure and environmental variability on the evolution

of microbial populations is therefore an important research avenue with many open questions. Here, we shed further light on the evolution of cooperative antimicrobial resistance by investigating an *in silico* metapopulation model of sensitive (S) and cooperative resistant (R) cells on a 2D grid of $L \times L$ demes connected through local migration at rate m . The metapopulation is subject to a constant antimicrobial input and time-fluctuating environmental conditions. These are modelled by the carrying capacity K of each deme switching back and forth between a high value ($K = K_+$, mild environment) and a much lower value ($K = K_- \ll K_+$, harsh environment) at a prescribed average rate ν (Fig. 1a). We find that for intermediate switching rate of K , $\nu \lesssim 1$ and for large environmental variability ($K_+/K_- \gg 1$), fluctuations cause the efficient clearance of resistance across the entire metapopulation when migration is slow to moderate, with the migration rate m not exceeding a critical value m_c (for $m < m_c$) that we have estimated analytically in Eq. (1). Slow migration, as is commonly used in microfluidic settings [47], is known to increase fragmentation and influences the evolution of the ensuing sub-populations [16, 49]. We show that, remarkably, slow but non-zero migration can enhance and accelerate the fluctuation-driven eradication of resistant cells ($m = 10^{-4} - 10^{-3}$ in Fig. 4, Extended Data Fig. 8, and Supplementary Section S3 Movie 2). Our results therefore demonstrate the critical and counterintuitive role of spatial migration that, jointly with environmental variability and demographic fluctuations, determines the maintenance or extinction of cooperative antimicrobial resistance.

Every time the environment suddenly switches from mild to harsh in the intermediate switching regime ($\nu \lesssim 1$), the carrying capacity changes from K_+ to K_- and all demes experience a population bottleneck. When $K_+/K_- \gg 1$, the bottleneck is strong (high environmental variability) and resistant cells are prone to extinction. Demographic fluctuations thus cause R eradication in some demes randomly distributed across the grid (Figs. 1b and 3e,g, Methods, Supplementary Section S3 Movie 3). Critically, resistant cells can migrate and recolonise R -free demes before the next bottleneck occurs, thereby locally reinstating resistance and preventing its global extinction (Figs. 1b and 3b,f,h). When migration is fast enough ($m > m_c$), resistant cells can recolonise more demes than are cleared of R cells by the compounded effects of bottlenecks and demographic fluctuations, and antimicrobial resistance thus survives across the metapopulation. For perfectly isolated demes ($m = 0$), R bacteria cannot recolonise resistant-free demes, and fast resistance extinction is most probable when K_+/K_- is at least of the order of the cooperation threshold N_{th} ($K_+/K_- \gtrsim N_{\text{th}}$) [26] (Fig. 2b-c). Surprisingly, the eradication of resistant cells from the entire metapopulation can be most efficient at slow but non-zero migration, when the R strain is eliminated with a probability close to 1, higher than in the absence of migration (Fig. 4c-f). This stems from R cells having a small chance to take over a deme whenever it experiences the harsh environment (where $K = K_-$) (Methods, Supplementary Section S2). Once this happens, in the absence of migration, resistance survives in any R -only deme (Extended Data Fig. 8b, Supplementary Section S3 Movie 1). However, when cells migrate at a slow rate m , S can recolonise all demes and the fluctuation-driven eradication mechanism may eliminate all resistance (Methods and Extended Data Fig. 8, Supplementary Section S3 Movie 2).

The impact of migration on the eradication of R cells is particularly significant when mK_+ (rate of cell migration per deme in the mild environment) is comparable to the frequency at which bottlenecks arise, yielding the condition $mK_+ \gtrsim \nu$ (Methods and Extended Data Fig. 8c). The probability of eradicating resistant cells in the intermediate switching regime, when $K_+/K_- \gtrsim N_{\text{th}}$, is close to 1 when the migration rate satisfies

$$\nu/K_+ \lesssim m \lesssim m_c \quad (3)$$

(golden and green lines in Fig. 4d-e), corresponding to near-optimal migration rates $m \sim 10^{-4} - 10^{-3}$ in Fig. 4f, which are of the same order as those in typical microfluidic experiments [47]. Remarkably, this demonstrates how migration can be instrumental in eradicating resistance when the environment varies neither too quickly nor too slowly and environmental variability is high. Eventually, after undergoing sufficiently many bottlenecks, the entire red phase in the heatmaps of the probability of R extinction (Fig. 4a-e and Extended Data Fig. 7, Supplementary Fig. S3) becomes fully dark (not shown), corresponding to an R eradication probability 1 for $0 < m \lesssim m_c$ (for $m = 0$ see Discussion and Extended Data Fig. 8b, Supplementary Section S3 Movie 1). Moreover, we predict that when the population is subject to extreme bottlenecks, $K_+/K_- \gtrsim N_{\text{th}}L^2$ (extreme environmental variability) and $\nu \lesssim 1$, resistance is doomed to go extinct regardless of the migration rate (Methods).

There are different ways of modelling cells' dispersal and migration in microbial populations. Cellular movement is often directed towards areas that are rich in resources [50], but dispersal is commonly

assumed to happen with a constant per capita migration rate, e.g., [18, 20]. We are here considering a more general density-dependent form of dispersal (Methods), positing that cells tend to migrate away towards a neighbouring patch when the resident deme occupancy is close to the carrying capacity K (lack of resources), whereas they are less likely to disperse when the local occupancy is well below K (abundance of resources). We have also considered the simpler form of dispersal where all cells can migrate onto a neighbouring deme with a constant per-capita rate m . For both types of migration, we have obtained similar results for the effects of spatial extension and fluctuations on the eradication of resistance (Extended Data Figs. 5 and 6, Supplementary Section S3 Movies 4-5). These additional data demonstrate that our findings are robust and qualitatively independent of the specific choice of how dispersal is implemented. Extending this work to species-specific or spatially dependent migration rates would be particularly relevant for complex metapopulation structure [15, 20].

In this study, we have specifically focused on a metapopulation model consisting of a 2D grid of $L \times L$ connected by cell migration (Fig. 1b, Methods). This is a natural setting to model microbial communities living on surfaces where cellular migration takes place, with possible applications ranging from the human skin [6], to the digestive tract [7] and plant leaf surfaces [4], the seabed [2], and general wet surfaces [3]. While the results presented here are specific to the above 2D metapopulation model, our main findings on the fluctuation-driven eradication of resistance under slow migration and intermediate switching rate are expected to hold also for other metapopulation structures, such as one-dimensional (1D) cycles or a three-dimensional (3D) lattice of demes. In fact, as long as environmental variability causes population bottlenecks and migration is responsible for the recolonisation of R -free demes, the same behaviour analysed here qualitatively holds independently of the space dimension. However, spatial migration being more limited in 1D than in 2D, we expect that near-optimal clearance of resistance would occur at higher migration rates on a cycle. For the same reasons, we expect that 3D fluctuation-driven resistance clearance should pertain at lower migration rates than in 2D. The impact of other spatial structures (such as star graphs, island models or cliques) has been studied for non-cooperative resistance, e.g., for constant environments and slow migration [18, 22], and under successive growth-and-dilution cycles coupled to fast cell migration [15, 20]. Understanding the impact of complex spatial structures on cooperative antimicrobial resistance remains mostly an open problem.

Our modelling approach is inspired by chemostat setups. These are commonly used in laboratory-controlled experiments to modulate the influx of nutrients and drugs. The concentration of resources and toxin can thus be set to impose harsh conditions that generate bottlenecks whose impact on the eco-evolutionary dynamics of bacterial populations can be studied [25, 51, 52]. We focus on the biologically relevant regime of intermediate environmental time variation [25, 44, 45], $\nu \lesssim 1$, for which the population size in each deme readily tracks the carrying capacity whereas the local S and R compositions relax more slowly, on a timescale of order $1/s$, with typically $s \sim 10^{-1}$ (Methods, Supplementary Section S1.1). This corresponds to environmental conditions changing from mild ($K = K_+$) to harsh ($K = K_-$) with a frequency once per hour/day, i.e. every 1 to 100 microbial generations (Methods), with the drug influx kept constant and environmental switches occurring rapidly (in < 1 less than one hour). These conditions are all feasible in the laboratory [25, 45], and can in principle be realised in a series of spatially connected chemostats, each acting as a deme, with the rate of cell migration set by the partial mixing between neighbouring demes-chemostats with fixed volumes. While we have conveniently represented the switching of the carrying capacity as random processes occurring at rates ν_{\pm} (Fig. 1a), an essentially equivalent practical implementation would let K vary periodically between K_+ and K_- with a period $1/\nu_+ + 1/\nu_-$ [39] (Methods, Supplementary Section S1.2).

We have carried out extensive stochastic simulations of the ensuing metapopulation dynamics, and repeatedly tracked the evolution of up to 10^7 microbes distributed across 400 spatial demes through hundreds of realisations, and thousands of different environmental parameters and migration rates (Methods). While this is a rather large metapopulation model, most experiments are carried out with bigger microbial populations [33, 53, 54]. We nevertheless expect that spatial fluctuation-driven eradication occurs also in large and more extended bacterial populations provided the conditions (2), which can be met in typical microbial communities (Methods), are actually satisfied. Moreover, with microfluidic devices and single-cell techniques, it is possible to perform spatially structured experiments with only 10 to 100 cells per ‘microhabitat patch’ [9, 47, 55], which are conditions compatible with our modelling parameters ($K_- = 80$).

It is worth noting that most laboratory experiments are carried out with batch cultures (growth-dilution cycles), e.g., [15, 56], which are easier to run than chemostat or microfluidic setups. However,

the concentration of nutrients (microbial consumption) and drug (enzymatic degradation by R cells) changes continuously in batch culture experiments, rendering their explicit modelling challenging [20, 57]. The 2D metapopulation considered here, when short periods in the harsh environment ($K = K_-$) are followed by extended sojourns in the mild environment ($K = K_+$), while the drug concentration would be assumed to remain roughly constant, may be viewed as approximately mimicking the growth-dilution cycles of batch cultures. The dynamic degradation of the drug can however play a critical role in the evolution of cooperative AMR, as shown in Ref. [21], where the fragmentation of the metapopulation into isolated demes enhances the maintenance of resistance.

While we have here focused on a two-strain metapopulation model, our main results can be extended to the eradication of resistant (R) cells from microbial populations consisting of multiple sensitive strains continuously experiencing mild and harsh environmental conditions in turn. To this end, the fraction of R cells in each deme should fluctuate about a low, non-zero value (here, $N_{\text{th}}/K_+ \ll 1$, Fig. 1). Additionally, the spatial fluctuation-driven eradication of resistance requires that the number of cells in each deme decreases sharply following a population bottleneck, while the deme composition evolves on a slower timescale, yielding a small R subpopulation prone to extinction in each deme. In our model, there are approximately $N_{\text{th}}K_-/K_+ \lesssim 1$ resistant cells in each deme after a bottleneck has occurred (Fig. 1, Methods). In the case of non-cooperative antimicrobial resistance, the fraction of resistant cells does not fluctuate about a small non-zero value, and the spread of sensitive bacteria is always hampered by the drug (Methods). Hence, in non-cooperative resistance, if there are initially sufficiently many R cells, resistance can take over the whole metapopulation [18, 20].

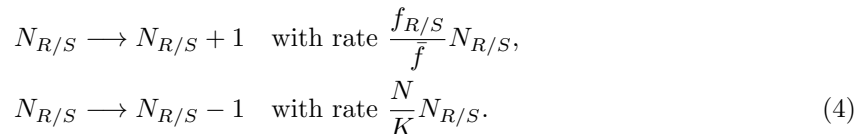
Environmental variations, spatial structure, cellular migration, and fluctuations are all ubiquitous key factors influencing the evolution of cooperative antimicrobial resistance. The joint effect of dispersal and fluctuations is particularly complex and poses a number of challenges [46, 48, 58]. In this study, we have demonstrated by theoretical and computational means that environmental variability and migration can lead to the efficient eradication of drug resistance from a 2D metapopulation. We have determined the origin and the near-optimal conditions for fluctuation-driven eradication of resistance in a spatial setting. To achieve this goal, the environment needs to change at an intermediate switching rate ($\nu \lesssim 1$), and environmental variability has to be strong enough ($K_+/K_- \gtrsim N_{\text{th}}$, assuming $N_{\text{th}} < K_- < K_+$) to generate a succession of population bottlenecks in each metapopulation deme where the local resistant population can be driven to extinction by demographic fluctuations. Resistant cells' migration can recolonise demes free of R cells, and hence often help maintain resistance. However, we have shown that strong bottlenecks may limit and effectively counter the recolonisation by dispersal. This results in a trade-off arising at $\nu/K_+ \lesssim m \lesssim m_c$, when slow but nonzero migration and sufficiently strong bottlenecks can act most synergistically to eradicate resistance by accelerating and enhancing the spatial fluctuation-driven eradication mechanism. We argue that these conclusions hold for microbial populations of realistic size and can be extended to other spatial structures. Our findings are robust against different forms of migration and are expected to hold for multi-strain communities. We have also discussed their relevance to batch cultures and propose feasible laboratory experiments [25, 51, 52]. We believe that our work can inform novel treatment protocols and pave the way to explore innovative alternative treatment options to prevent the spread of antimicrobial resistance in clinical and other applications.

4 Methods & Model

4.1 Microbial model for an isolated deme

A common mechanism of antimicrobial resistance is based on *drug exposure protection*. Usually, it involves resistant cells investing metabolic resources to produce enzymes that hydrolyse antimicrobial drugs [42, 59, 60]. An example is the inactivation of the broad class of β -lactam antibiotics by the β -lactamase enzyme [43] that is often produced by resistant cells carrying gene-bearing plasmids commonly used in laboratory experiments [42, 61]. This resistance mechanism can lead to a form of AMR cooperative behaviour when drug-sensitive cells are protected from the toxin without paying any metabolic cost. Inspired by β -lactamase AMR, we here assume that each R cell produces the resistance enzyme at a fixed rate. The associated extra metabolic cost reduces the R growth rate and hence lowers the resistant cells' fitness f_R from its baseline value set to 1. Assuming that resistance entails a constant fitness cost $s > 0$, the R fitness is set as $f_R = 1 - s > 0$ regardless of the local drug

concentration. When sensitive bacteria are not exposed to the toxin, they grow faster than R cells and have a baseline fitness $f_S = 1$ higher than f_R (no extra metabolic cost for S). However, the spread of S cells is hindered when they are in contact with the drug, and their fitness is then reduced to $f_S = 1 - a < f_R$. Sensitive bacteria recover the baseline fitness $f_S = 1$ when the number of R microbes N_R reaches the *cooperation threshold* N_{th} . When $N_R \geq N_{\text{th}}$, the resistance enzyme concentration in a deme is sufficiently high to locally protect all microbes from the toxin [26, 28, 42, 59, 60] (Fig. 1a). This scenario models the effect of biostatic antimicrobial drugs at low concentration in demes/chemostats whose volume is kept constant, a regime in which the action of biocidal and biostatic toxins is similar [62, 63]. The per-capita death rate of any cell in a deme is N/K , where $N = N_R + N_S$ is the population size in the deme and K denotes the same carrying capacity of each deme. The composition of each deme evolves stochastically according to the microbial birth and death reactions



Here, the R/S birth rate in a deme is given by the fitness $f_{R/S}$ relative to the average fitness in the deme $\bar{f} = (f_R N_R + f_S N_S)/N$ [26, 27, 28, 37, 38, 39]. The choice $f_{R/S}/\bar{f}$ for the birth rate allows us to establish a relationship with the well-known Moran process, a reference model in mathematical biology [26, 37, 38, 64, 65]. The master equation of this multivariate continuous-time birth-death process is given in the Supplementary Information (Supplementary Section S1.3). The resulting eco-evolutionary dynamics is characterised by a fast dynamics of the total number of microbes in each deme, N , that is driven by the fluctuating carrying capacity K and reaches a quasi-stationary distribution after very few microbial generations, i.e. on a ecological timescale ~ 1 (Supplementary Fig. S1 and Supplementary Section S1.2). Since $s \lesssim 1$, the fraction of R and S cells composing a deme evolves on a slower evolutionary timescale $\sim 1/s$ (at rate $f_S - f_R \sim s$). We note that the intermediate environmental switching regime mentioned previously, see, e.g., Eq. (2), refers to an average switching rate $\nu \sim s \lesssim 1$. In a static environment, the number of R cells fluctuates about the cooperation threshold $N_R \approx N_{\text{th}}$, while there are $N_S \approx K - N_{\text{th}}$ sensitive cells (Fig. 1a; Supplementary Fig. S2 and Supplementary Section S2). In our examples, we have chosen a realistic small value $s = 0.1$ for the extra metabolic cost associated with resistance, and a plausible reduction of 25% of f_S , with $a = 0.25$, when S cells are exposed unprotected to the drug [63, 66, 67]. These values are indicative, but we expect that the results reported here should qualitatively hold for a broad range of parameters [26].

4.2 Environmental dynamics

Environmental variability, random or periodic, refers to changes in external conditions that are ubiquitous and commonly arise at the microscale. Variations of the environment shape microbial populations by coupling their ecological and evolutionary dynamics (eco-evolutionary dynamics) [23], e.g., the changes in the size and composition of a population in a deme are dynamically interdependent [24, 68]. The amplitude of demographic fluctuations is modulated by environmental variability, and this coupling is particularly important in small populations [23, 24, 37, 38, 39, 40, 41, 69]. Here we wish to model continuous sudden and drastic environmental changes, like the occurrence of regular population bottlenecks. To this end, we assume that a random telegraph process $\xi(t) \in \{-1, 1\}$ drives the carrying capacity $K(t)$ of each deme. The coloured dichotomous Markov noise ξ switches back and forth according to $\xi \rightarrow -\xi$ at rate ν_{\pm} when $\xi = \pm 1$ [70, 71]. Environmental variability is thus modelled by writing the *time-dependent* carrying capacity as [26, 27, 28, 37, 38, 39, 40, 41, 69]

$$K(t) = \frac{1}{2} [K_+ + K_- + \xi(t) (K_+ - K_-)], \quad (5)$$

with K switching back and forth from K_+ when the environment is mild ($\xi = 1$) to $K_- < K_+$ in a harsh environment ($\xi = -1$) at rate ν_{\pm} [26, 27, 28, 37, 38, 39, 40, 41, 69, 70, 71, 72] (Fig. 1a), according to

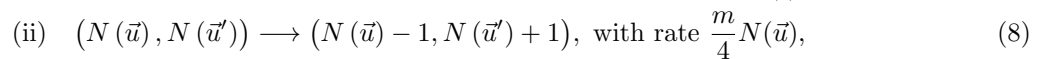
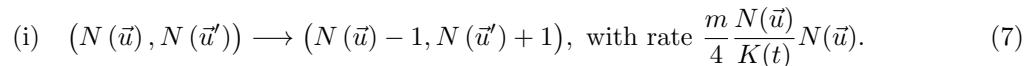


For our analysis, it is convenient to introduce the mean switching rate $\nu = (\nu_- + \nu_+)/2$, and the switching bias $\delta = (\nu_- - \nu_+)/(\nu_- + \nu_+)$, where $|\delta| \leq 1$, and $\delta > 0$ when more time is spent on average

in the mild environment. The stationary population distribution in each deme can be approximated analytically by focusing on the fluctuating carrying capacity (5). It is bimodal with peaks at K_+ and K_- ($N \approx K_{\pm}$) when the environment varies very slowly, $\nu \ll 1$. When $\nu \gg 1$, the environment varies very quickly and N is unimodally distributed around its peak at $N \approx 2K_+K_- / [(1-\delta)K_+ + (1+\delta)K_-]$ [26, 39] (Supplementary Fig. S2 and Supplementary Section S1.2). When $\nu \sim s$, the population size in each deme tracks the carrying capacity, and a population bottleneck arises each time the carrying capacity switches from K_+ to K_- , which occurs at an average frequency $\nu_+ \nu_- / (2\nu) = \nu(1-\delta^2)/2$. Modelling environmental changes using the telegraph process is a natural and simple choice. We note that dichotomous noise is simple to simulate, amenable to mathematical analysis (Supplementary Section S1.2), and it can naturally describe the binary fluctuating environmental conditions that are commonly used in laboratory-controlled experiments [25, 45, 51, 52]. While more complex forms of noise can be considered, the choice made here is therefore biologically relevant and convenient (Supplementary Section S1.2).

4.3 Spatial structure and cell migration

Microbial populations generally evolve in spatially structured environments in which cells can migrate [73, 74]. Spatial migration can be coupled to ecological changes and evolutionary dynamics [15, 21, 22], and is generally thought to moderate local fluctuations, with higher migration between sites homogenizing the local population composition [58]. Here, we study a metapopulation embedded in a 2D spatial grid of $L \times L$ demes (with periodic boundary conditions) modelling a surface-attached microbial population [2, 3, 4, 6, 7] (Fig. 1b). These are connected by cell migration between neighbouring sites. In our study, we have considered two forms of migration: (i) We have assumed that all cells in a deme \vec{u} have a density-dependent per-capita migration rate $mN(\vec{u})/K(t)$, which increases as the deme's population size $N(\vec{u})$ approaches the carrying capacity, i.e., when available resources are subject to local constraints. (ii) We have also considered the simpler form of migration where all cells in a deme \vec{u} feature the same constant per capita migration rate m (Extended Data Fig. 6 and Supplementary Section S3 Movie 5). We represent these two forms of migration by picking randomly a cell (either R or S) from deme \vec{u} and moving it into a nearest-neighbour \vec{u}' according to the following stochastic reactions:



where the destination deme \vec{u}' is randomly picked between the four nearest neighbours of \vec{u} . The results reported in Figs. 2, 3, and 4 were obtained with the density-dependent form of migration (7). However, we have confirmed that the specific form of migration does not qualitatively affect our findings for the fluctuation-driven eradication of resistance at intermediate environmental switching rates, as demonstrated by the comparison of Extended Data Figs. 5 and 6 (Discussion, Supplementary Section S3 Movies 4-5).

Since most migrations occur when the population resides in the mild environmental state where $K = K_+$ and the number of microbes in each deme is typically large, we can estimate the rate of migration per deme in the intermediate switching regime (where $\nu \sim s$) as mK_+ . The impact of migration on microbial dynamics is most striking when there is at least one cell migrating into each deme between consecutive bottlenecks. Matching the rates at which these events occur yields $m \gtrsim \nu/K_+$. Migration rates lower than ν/K_+ (i.e. $m < 10^{-3.5}$ in Fig. 2 and $m < 10^{-4.5}$ in Fig. 4) lead to the same probability of R eradication as $m = 0$, whereas migration efficiently rescues resistance when $m > m_c$, see Eq. (1). The master equation of the full metapopulation model with migration and switching carrying capacity in each deme is given in Supplementary Section S1.3.

4.4 Fluctuation-driven eradication mechanism with spatial migration

Fluctuation-driven eradication of resistance in a deme arises when the carrying capacity switches between K_+ and K_- at rate $\nu \sim s$, generating strong enough population bottlenecks ($K_+/K_- \gtrsim N_{\text{th}}$). In this regime, the number of microbes in the deme continuously tracks the carrying capacity, while the deme's composition evolves on a slower timescale $\sim 1/s$. After each bottleneck, the fraction of

R cells in the deme initially fluctuates about $N_{\text{th}}/K_+ \ll 1$, and their expected number in the harsh environment, $N_R \approx N_{\text{th}}K_-/K_+ \lesssim 1$, is sufficiently low for demographic fluctuations to effect the eradication of resistance [26].

Hence, we assume that approximately K_- cells are randomly drawn to survive a bottleneck. Given that the number of cells before the bottleneck is sufficiently high ($K_+ \gg 1$), each R cell survives with the same independent probability (random draws with replacement), which matches the fraction of R cells, that is approximately N_{th}/K_+ . Therefore, the number of R cells surviving one bottleneck can be drawn from a Poisson distribution of mean $N_{\text{th}}K_-/K_+$, and the probability that one bottleneck eradicates resistance yields $\exp\left(-\frac{N_{\text{th}}K_-}{K_+}\right)$. In this regime, the fluctuation-driven clearance of AMR is attempted at each bottleneck (Fig. 1a). AMR fluctuation-driven eradication thus occurs at a rate comparable to the bottleneck frequency, given by $\frac{\nu-\nu_+}{2\nu} = \nu(1-\delta^2)/2$. Consequently, the rate at which each deme becomes R -free is approximately $\frac{\nu-\nu_+}{2\nu} \exp\left(-\frac{N_{\text{th}}K_-}{K_+}\right)$.

The demes of the metapopulation are connected by cell migration, which generally homogenizes the local population composition [58] and here tends to favour the coexistence of R and S cells [46]. Noting that the fraction of demes where resistance survives a single bottleneck can be approximated by $1 - \exp\left(-\frac{N_{\text{th}}K_-}{K_+}\right)$, we can estimate that the total rate of resistant cells migrating from each of these demes is $mN_{\text{th}} \left[1 - \exp\left(-\frac{N_{\text{th}}K_-}{K_+}\right)\right]$. Matching this rate of migration of R cells with the rate at which a deme becomes R -free, $\frac{\nu-\nu_+}{2\nu} \exp\left(-\frac{N_{\text{th}}K_-}{K_+}\right)$, we obtain the critical migration rate m_c .

When $m \gg m_c$, see Eq. (1), numerous cells migrate between successive bottlenecks. This efficiently mixes up the local population composition, and helps maintain resistance by recolonising R -free demes (Fig. 1b, Extended Data Fig. 8d). However, when $\nu/K_+ \lesssim m \lesssim m_c$, the rate of cell migration per deme is comparable to the bottleneck frequency, and migration thus enhances and speeds up the eradication of resistance (Discussion, Fig. 4). When $\nu/K_+ \lesssim m \lesssim m_c$ and $\nu \sim s$, sensitive cells can recolonise any R -only deme, and resistant cells are prone to be driven to extinction by fluctuations (Fig. 1b and Extended Data Fig. 8c). For this spatial fluctuation-driven eradication mechanism to work efficiently, the rate of environmental variability should neither be too low, ensuring that recolonisation does not reinstate resistance, nor too high in order to guarantee the production of bottlenecks, and more time be spent in the mild environment (on average) for coexisting demes to consist overwhelmingly of S cells when bottlenecks occur. We have thus found that the frequencies in the range $s/10 \leq \nu \leq 10s$ and a switching bias $\delta \geq 0$ ($0.01 \leq \nu \leq 1$, $0 \leq \delta \leq 0.90$ in Extended Data Fig. 7 and Supplementary Fig. S3) optimise the spatial fluctuation-driven eradication of resistance. Slow migration is most effective in speeding up and enhancing the fluctuation-driven clearance of R cells when $\nu \sim s$ and $\delta > 0$ (Extended Data Fig. 7; Supplementary Fig. S3; and Supplementary Section S3 Movies 1-3). In the limit of very fast migration, $m \gg 1$, the metapopulation can be regarded as L^2 fully connected demes (island model [75, 76]), all subject to the same fluctuating carrying capacity $K(t)$. In this case, the fraction of R cells just after an environmental bottleneck still fluctuates about N_{th}/K_+ in each of the fully connected sites, all experiencing the carrying capacity K_- . The approximate total number of R cells across the metapopulation right after a bottleneck is thus $L^2 N_{\text{th}}K_-/K_+$. When $m \gg 1$, resistance can typically be eradicated if all R cells are eliminated simultaneously during a single bottleneck. This can occur when the expected total number of R cells after a bottleneck is of order 1, i.e., for very strong bottlenecks $K_+/K_- \gtrsim N_{\text{th}}L^2$. Hence, when $\nu \sim s$ and $m \gg 1$, fluctuation-driven eradication of resistance occurs for very strong bottlenecks, $K_+/K_- \gtrsim N_{\text{th}}L^2$, independent of the actual value of m .

Finally, we expect that the above fluctuation-driven eradication of AMR in spatially structured environments holds when conditions (2) are satisfied by the typically big microbial populations found in nature [33, 53, 54], e.g., $(K_+, K_-, N_{\text{th}}) \sim (10^{11}, 10^6, 10^5)$.

4.5 Computational methods

In this section, we explain how the extensive stochastic simulations of the metapopulation dynamics were performed and summarise the parameters that we have used.

4.5.1 Metapopulation simulations

A natural extension to the non-spatial model of a well-mixed microbial community is through agent-based lattice simulations. This work employs a stochastic Monte Carlo algorithm on a two-dimensional, $L \times L$, square lattice (metapopulation) with periodic boundary conditions to investigate interaction effects of diffusively-coupled neighbouring microbial communities. The Gillespie algorithm [77] was also considered, but due to the amount of cells within each deme and overall size of the metapopulation, it was deemed less computationally efficient. Each microbial community (deme) within the lattice contains sensitive and resistant cells whose populations are governed by a birth-death process with migration and are subject to a fluctuating carrying capacity, according to (4)-(8). To minimize initial transients, at $t = 0$ a total of $N_{\text{th}}L^2$ resistant and $(K - N_{\text{th}})L^2$ sensitive cells (with $K \in \{K_-, K_+\}$) are uniformly distributed at random among all L^2 demes in the metapopulation. The expected initial number of resistant and sensitive cells here matches their respective stationary population in a static environment, $N_R^0 = N_{\text{th}}$ and $N_S^0 = K - N_{\text{th}}$ (Methods). Further, the environmental state of the metapopulation at $t = 0$ begins at stationarity, $K(t = 0) = \langle K(t) \rangle = \frac{1}{2} [K_+ + K_- + \delta(K_+ - K_-)]$ with the mean of the dichotomous Markov noise equalling that of the environmental switching bias, $\langle \xi(t) \rangle = \delta$ [26, 39]. Thus, the system begins in a harsh (K_-) or mild (K_+) environment with a probability of $(1 - \delta)/2$ or $(1 + \delta)/2$, respectively. We ran 200 realisations for each parameter set of Figs. 2 and 4, Extended Data Fig. 5, and panels e and g of Extended Data Fig. 7, and ran 50 realisations for each parameter set in Extended Data Fig. 6 and all panels of Extended Data Fig. 7 (except for panels e and g). Each panel of Fig. 3 features the same single simulation realisation. Results reported in Fig. 1a (bottom) and Extended Data Fig. 8a for the dynamics in a single isolated deme were obtained using the classical Gillespie algorithm [77].

The system evolves in time units of microbial generations, where we consider one generation to equal one Monte Carlo Step (MCS), e.g., bacteria replicate on a scale of roughly once every ~ 1 hour. Within every generation, the environment can switch at rate ν and cells are chosen at random to attempt birth, death, or migration reactions as described by Eqs. (4), (7), and (8). We have used two forms of migration: one where the per capita migration rate depends on the deme's local population density, Eq. (7), and a simpler case where that rate is constant, Eq. (8). Migration has been implemented in the same way for both formulations. A single MCS is said to be completed once the number of attempted death or birth reactions equals twice the current number of cells within the system, $1 \text{ MCS} = 2 \sum_{\vec{u}} (N_S(\vec{u}) + N_R(\vec{u}))$ where the sum is over all the demes, \vec{u} .¹ Therefore, on average, each cell in the system attempts either one birth or one death reaction within a generation. Since the simulation time unit is set as one microbial generation, migration reactions and environmental switches do not contribute to the above reaction count. This allows for a direct comparison between simulations at different migration m and environmental rates ν . For all finite stochastic systems with an absorbing state, the final equilibrium corresponds to the absorption in that state. In our model, the ultimate absorbing state is characterised by the total extinction of both microbial strains. However, this is unobservable in a reasonable amount of computational time (or in real microbial communities) as this phenomenon occurs on a timescale that diverges dramatically with the total population and the size of the grid of demes. In our study, we ran simulations for up to 500 generations, which is of the order of 10^2 experimental hours. This is sufficiently long to observe the fluctuation-driven eradication of R cells in the metapopulation (when feasible), but short enough to maintain computational efficiency.

4.5.2 Simulation parameters

To run a single simulation, 12 parameters are specified: the side length of the square lattice of demes, L ; the duration of the simulation (number of microbial generations), t_{max} ; the average initial number of sensitive and resistant cells per deme at $t = 0$, N_S^0 and N_R^0 ; the impact of the drug on the fitness of exposed sensitive cells, a ; the constant metabolic cost for resistant cells to generate the resistance enzyme, s ; the migration rate, m ; the mild and harsh carrying capacity in each deme, K_+ and K_- ; the resistant cooperation threshold, N_{th} ; the average environmental switching rate, ν ; and the environmental bias, δ . Throughout this work, we fixed seven parameters in all lattice simulations for computational convenience: $L = 20$, $t_{\text{max}} = 500$, $N_R^0 = 40 = N_{\text{th}}$, $a = 0.25$, $s = 0.1$, and $K_- = 80$. The remaining parameters are specified within the figure captions. All parameters are summarised in Ex-

¹There are $\sim 10^4$ birth/death events in 1 MCS when $N(\vec{u}) = N_S(\vec{u}) + N_R(\vec{u}) \approx K_-$ in each deme \vec{u} , and $\sim 10^5 - 10^7$ events when $N(\vec{u}) \approx K_+$.

tended Data Table 1. In our figures, we have explored and characterised the spatial fluctuation-driven eradication of R across the two-dimensional metapopulation by tuning the average switching rate ν , the environmental switching bias δ determining the relative time spent in mild/harsh conditions, the migration rate m , and the bottleneck strength K_+/K_- (keeping K_- fixed).

The explored range of migration rates varies from small to large migration values, $m \in [10^{-5}, 10^{-1}]$, as well as the case of absent migration, $m = 0$ (separated by vertical dashed white lines in Figs. 2 and 4, Extended Data Fig. 7, and Supplementary Fig. S3). We simulated a range of values of the demes' carrying capacity K_+ in the mild environment, with K_+ spanning from 10^3 to $3.2 \cdot 10^4$. The environmental bottleneck strength K_+/K_- thus ranged from 12.5 to 400. The upper limit in K_+ and the side length of the square grid L set the maximum total number of cells across the grid of demes ($\sim L^2 K_+$), which was bounded by $\sim 10^7$ due to computational constraints (Discussion). We also tested an extended range of intermediate environmental switching parameters to corroborate our results, with $\nu \in \{0.01, 0.1, 1\}$ and $\delta \in \{0.25, 0.5, 0.75\}$ (Extended Data Fig. 7; see Supplementary Fig. S3 for additional slow and fast switching environments).

5 Data availability

The data generated and used within this work can be found at the Open Science Framework repository (Lluís Hernández-Navarro, Kenneth Distefano, Uwe C. Täuber, and Mauro Mobilia. 2024. Supplementary data, code, and videos for "Slow spatial migration can help eradicate cooperative antimicrobial resistance in time-varying environments". OSF. <https://doi.org/10.17605/OSF.IO/EPB28>).

6 Code availability

The C++ code used to generate the data and the Python and Matlab codes to process and visualize the data within this work can be found at the Open Science Framework repository (Lluís Hernández-Navarro, Kenneth Distefano, Uwe C. Täuber, and Mauro Mobilia. 2024. Supplementary data, code, and videos for "Slow spatial migration can help eradicate cooperative antimicrobial resistance in time-varying environments". OSF. <https://doi.org/10.17605/OSF.IO/EPB28>).

Acknowledgements

The authors would like to thank M. Asker, J. Jiménez, S. Muñoz Montero, M. Pleimling, A. M. Rucklidge, and M. Swailem for fruitful discussions. L. H. N. and M. M. gratefully acknowledge funding from the U.K. Engineering and Physical Sciences Research Council (EPSRC) under the Grant No. EP/V014439/1 for the project 'DMS-EPSRC Eco-Evolutionary Dynamics of Fluctuating Populations' (<https://eedfp.com/>). K. D. and U. C. T.'s contribution to this research was supported by the U.S. National Science Foundation, Division of Mathematical Sciences under Award No. NSF DMS-2128587.

Author contributions

L.H.-N. and M.M. designed the project. L.H.-N., K.D., and M.M. analysed the results. K.D. performed the simulations. K.D. and L.H.-N. prepared the figures. M.M. and U.C.T. supervised the study. L.H.N., M.M., and K.D. wrote and revised the manuscript with input from U.C.T.

Correspondence

Correspondence and requests for materials should be addressed to [Lluís Hernández-Navarro](#) or [Mauro Mobilia](#).

References

- [1] S. Bickel and D. Or. Soil bacterial diversity mediated by microscale aqueous-phase processes across biomes. *Nat. Commun.*, 11(1):116, 2020.
- [2] L. M. Dann, J. G. Mitchell, P. G. Speck, K. Newton, T. Jeffries, and J. Paterson. Virio-and bacterioplankton microscale distributions at the sediment-water interface. *PLoS One*, 9(7):e102805, 2014.
- [3] M. Grinberg, T. Orevi, S. Steinberg, and N. Kashtan. Bacterial survival in microscopic surface wetness. *eLife*, 8:e48508, 2019.
- [4] J.-M. Monier and S. E. Lindow. Frequency, size, and localization of bacterial aggregates on bean leaf surfaces. *Appl. Environ. Microbiol.*, 70(1):346–355, 2004.
- [5] J. L. Mark Welch, Y. Hasegawa, N. P. McNulty, J. I. Gordon, and G. G. Borisy. Spatial organization of a model 15-member human gut microbiota established in gnotobiotic mice. *PNAS*, 114(43):9105–9114, 2017.
- [6] A. Conwill, A. C. Kuan, R. Damerla, A. J. Poret, J. S. Baker, A. D. Tripp, E. J. Alm, and T. D. Lieberman. Anatomy promotes neutral coexistence of strains in the human skin microbiome. *Cell Host Microbe*, 30(2):171–182, 2022.
- [7] J.-J. She, W.-X. Liu, X.-M. Ding, G. Guo, J. Han, F.-Y. Shi, H. C.-H. Lau, C.-G. Ding, W.-J. Xue, W. Shi, et al. Defining the biogeographical map and potential bacterial translocation of microbiome in human ‘surface organs’. *Nat. Commun.*, 15(1):427, 2024.
- [8] O. X. Cordero and M. S. Datta. Microbial interactions and community assembly at microscales. *Curr. Opin. Microbiol.*, 31:227–234, 2016.
- [9] R. H. Hsu, R. L. Clark, J. W. Tan, J. C. Ahn, S. Gupta, P. A. Romero, and O. S. Venturelli. Microbial interaction network inference in microfluidic droplets. *Cell Syst.*, 9(3):229–242, 2019.
- [10] N. Mahrt, A. Tietze, S. Künzel, S. Franzenburg, C. Barbosa, G. Jansen, and H. Schulenburg. Bottleneck size and selection level reproducibly impact evolution of antibiotic resistance. *Nat. Ecol. Evol.*, 5(9):1233–1242, 2021.
- [11] F. Wu, Y. Ha, A. Weiss, M. Wang, J. Letourneau, S. Wang, N. Luo, S. Huang, C. T. Lee, L. A. David, et al. Modulation of microbial community dynamics by spatial partitioning. *Nat. Chem. Biol.*, 18(4):394–402, 2022.
- [12] J. R. Nahum, P. Godfrey-Smith, B. N. Harding, J. H. Marcus, J. Carlson-Stevermer, and B. Kerr. A tortoise–hare pattern seen in adapting structured and unstructured populations suggests a rugged fitness landscape in bacteria. *PNAS*, 112(24):7530–7535, 2015.
- [13] A. Limdi, A. Pérez-Escudero, A. Li, and J. Gore. Asymmetric migration decreases stability but increases resilience in a heterogeneous metapopulation. *Nat. Commun.*, 9(1):2969, 2018.
- [14] S. Gokhale, A. Conwill, T. Ranjan, and J. Gore. Migration alters oscillatory dynamics and promotes survival in connected bacterial populations. *Nat. Commun.*, 9(1):5273, 2018.
- [15] P. P. Chakraborty, L. R. Nemzer, and R. Kassen. Experimental evidence that network topology can accelerate the spread of beneficial mutations. *Evol. Lett.*, 7(6):447–456, 2023.
- [16] J. Kreger, D. Brown, N. L. Komarova, D. Wodarz, and J. Pritchard. The role of migration in mutant dynamics in fragmented populations. *J. Evol. Biol.*, 36(2):444–460, 2023.
- [17] B. Allen, G. Lippner, Y.-T. Chen, B. Fotouhi, N. Momeni, S.-T. Yau, and M. A. Nowak. Evolutionary dynamics on any population structure. *Nature*, 544(7649):227–230, 2017.
- [18] L. Marrec, I. Lamberti, and A.-F. Bitbol. Toward a universal model for spatially structured populations. *Phys. Rev. Lett.*, 127(21):218102, 2021.

- [19] S. Yagoobi and A. Traulsen. Fixation probabilities in network structured meta-populations. *Sci. Rep.*, 11(1):17979, 2021.
- [20] A. Abbara and A.-F. Bitbol. Frequent asymmetric migrations suppress natural selection in spatially structured populations. *PNAS nexus*, 2(11):392, 2023.
- [21] N. Verdon, O. Popescu, S. Titmuss, and R. J. Allen. Habitat fragmentation enhances microbial collective defence. *bioRxiv*, 2024.03.20.585867, 2024.
- [22] C. Fruet, E. L. Müller, C. Loverdo, and A.-F. Bitbol. Spatial structure facilitates evolutionary rescue by cost-free drug resistance. *arXiv*, 2409.07377, 2024.
- [23] F. Pelletier, D. Garant, and H. P. Hendry. Eco-evolutionary dynamics. *Phil. Trans. R. Soc. B*, 364:1483, 2009.
- [24] K. I. Harrington and A. Sanchez. Eco-evolutionary dynamics of complex strategies in microbial communities. *Commun. Integr. Biol.*, 7(1):e28230, 2014.
- [25] F. Abdul-Rahman, D. Tranchina, and D. Gresham. Fluctuating environments maintain genetic diversity through neutral fitness effects and balancing selection. *Mol. Biol. Evol.*, 38(10):4362–4375, 2021.
- [26] L. Hernández-Navarro, M. Asker, A. M. Rucklidge, and M. Mobilia. Coupled environmental and demographic fluctuations shape the evolution of cooperative antimicrobial resistance. *J. R. Soc. Interface*, 20(208):20230393, 2023.
- [27] M. Asker, L. Hernández-Navarro, A. M. Rucklidge, and M. Mobilia. Coexistence of competing microbial strains under twofold environmental variability and demographic fluctuations. *New J. Phys.*, 25(12):123010, 2023.
- [28] L. Hernández-Navarro, M. Asker, and M. Mobilia. Eco-evolutionary dynamics of cooperative antimicrobial resistance in a population of fluctuating volume and size. *J. Phys. A: Math. Theor.*, 57(26):265003, 2024.
- [29] B. A. Adamie, H. T. Akwar, M. Arroyo, H. Bayko, M. Hafner, S. Harrison, M. Jeannin, D. King, S. Kweon, N. D. Kyeong, F. Olumogba, I. Rigby, S. J. Song, E. Yerushalmi, J. Yugueros-Marcos, and S. Zakaria. Forecasting the fallout from AMR: Economic impacts of antimicrobial resistance in food-producing animals. *Rep. EcoAMR Ser.*, 2024.
- [30] S. E. Vollset, U. Altay, N. V. Bhattacharjee, J. Chalek, K. Giannakis, A. Gray, C. Han, P. A. Lindstedt, M. Naghavi, C. Raggi, A. E. Smith, G. Smith, L. Swetschinski, E. Wool, C. W. Yuan, and C. J. L. Murray. Forecasting the fallout from AMR: Human health impacts of antimicrobial resistance. *Rep. EcoAMR Ser.*, 2024.
- [31] M. Naghavi, S. E. Vollset, K. S. Ikuta, L. R. Swetschinski, A. P. Gray, E. E. Wool, G. R. Aguilar, T. Mestrovic, G. Smith, C. Han, et al. Global burden of bacterial antimicrobial resistance 1990–2021: a systematic analysis with forecasts to 2050. *Lancet*, 404(10459):1199–1226, 2024.
- [32] W. Hengzhuang, H. Wu, O. Ciofu, Z. Song, and N. Høiby. In vivo pharmacokinetics/pharmacodynamics of colistin and imipenem in pseudomonas aeruginosa biofilm infection. *Antimicrob. Agents Chemother.*, 56(5):2683–2690, 2012.
- [33] J. Coates, B. R. Park, D. Le, E. Şimşek, W. Chaudhry, and M. Kim. Antibiotic-induced population fluctuations and stochastic clearance of bacteria. *eLife*, 7:e32976, 2018.
- [34] D. G. Larsson and C.-F. Flach. Antibiotic resistance in the environment. *Nat. Rev. Microbiol.*, 20(5):257–269, 2022.
- [35] N. M. Vega and J. Gore. Collective antibiotic resistance: mechanisms and implications. *Curr. Opin. Microbiol.*, 21:28–34, 2014.
- [36] L. M. Wahl, P. J. Gerrish, and I. Saika-Voivod. Evaluating the impact of population bottlenecks in experimental evolution. *Genet.*, 162:961, 2002.

- [37] K. Wienand, E. Frey, and M. Mobilia. Evolution of a fluctuating population in a randomly switching environment. *Phys. Rev. Lett.*, 119(15):158301, 2017.
- [38] K. Wienand, E. Frey, and M. Mobilia. Eco-evolutionary dynamics of a population with randomly switching carrying capacity. *J. R. Soc. Interface*, 15(145):20180343, 2018.
- [39] A. Taitelbaum, R. West, M. Assaf, and M. Mobilia. Population dynamics in a changing environment: random versus periodic switching. *Phys. Rev. Lett.*, 125(4):048105, 2020.
- [40] A. Taitelbaum, R. West, M. Mobilia, and M. Assaf. Evolutionary dynamics in a varying environment: Continuous versus discrete noise. *Phys. Rev. Res.*, 5(2):L022004, 2023.
- [41] S. Shibasaki, M. Mobilia, and S. Mitri. Exclusion of the fittest predicts microbial community diversity in fluctuating environments. *J. R. Soc. Interface*, 18:20210613, 2021.
- [42] E. A. Yurtsev, H. X. Chao, M. S. Datta, T. Artemova, and J. Gore. Bacterial cheating drives the population dynamics of cooperative antibiotic resistance plasmids. *Mol. Syst. Biol.*, 9:683, 2013.
- [43] K. Bush and P. A. Bradford. β -lactams and β -lactamase inhibitors: an overview. *Cold Spring Harb. Perspect. Med.*, 6(8):a025247, 2016.
- [44] E. Santillan, H. Seshan, F. Constancias, D. I. Drautz-Moses, and S. Wuertz. Frequency of disturbance alters diversity, function, and underlying assembly mechanisms of complex bacterial communities. *NPJ Biofilms Microbi.*, 5:1–9, 2019.
- [45] J. Nguyen, J. Lara-Gutiérrez, and R. Stocker. Environmental fluctuations and their effects on microbial communities, populations and individuals. *FEMS Microbiol. Rev.*, 45:fuaa068, 2021.
- [46] S. Gude, E. Pince, K. M. Taute, A.-B. Seinen, T. S. Shimizu, and J. S. Tans. Bacterial coexistence driven by motility and spatial competition. *Nature*, 578:588–592, 2020.
- [47] J. E. Keymer, P. Galajda, C. Muldoon, S. Park, and R. H. Austin. Bacterial metapopulations in nanofabricated landscapes. *PNAS*, 103(46):17290–17295, 2006.
- [48] S. Widder, R. J. Allen, T. Pfeiffer, T. P. Curtis, C. Wiuf, W. T. Sloan, O. X. Cordero, S. P. Brown, B. Momeni, W. Shou, et al. Challenges in microbial ecology: building predictive understanding of community function and dynamics. *ISME J.*, 10:2557–2568, 2016.
- [49] M. Slatkin. Fixation probabilities and fixation times in a subdivided population. *Evol.*, 35:477–478, 1981.
- [50] J. M. Keegstra, F. Carrara, and R. Stocker. The ecological roles of bacterial chemotaxis. *Nat. Rev. Microbiol.*, 20(8):491–504, 2022.
- [51] M. Acar, J. Mettetal, and A. van Oudenaarden. Stochastic switching as a survival strategy in fluctuating environment. *Nat. Genet.*, 40:471–475, 2008.
- [52] G. Lambert and E. Kussell. Memory and fitness optimization of bacteria under fluctuating environments. *PLoS Genet.*, 10(9):e1004556, 2014.
- [53] W. E. Feldman. Concentrations of bacteria in cerebrospinal fluid of patients with bacterial meningitis. *J. Pediatr.*, 88(4):549–552, 1976.
- [54] M. Palaci, R. Dietze, D. J. Hadad, F. K. C. Ribeiro, R. L. Peres, S. A. Vinhas, E. L. N. Maciel, V. do Valle Dettoni, L. Horter, W. H. Boom, et al. Cavitory disease and quantitative sputum bacillary load in cases of pulmonary tuberculosis. *J. Clin. Microbiol.*, 45(12):4064–4066, 2007.
- [55] K. Totlani, J.-W. Hurkmans, W. M. van Gulik, M. T. Kreutzer, and V. van Steijn. Scalable microfluidic droplet on-demand generator for non-steady operation of droplet-based assays. *Lab Chip*, 20(8):1398–1409, 2020.
- [56] J. E. Goldford, N. Lu, D. Bajić, S. Estrela, M. Tikhonov, A. Sanchez-Gorostiaga, D. Segrè, P. Mehta, and A. Sanchez. Emergent simplicity in microbial community assembly. *Science*, 361:469, 2018.

- [57] A. Erez, J. G. Lopez, B. G. Weiner, Y. Meir, and N. S. Wingreen. Nutrient levels and trade-offs control diversity in a serial dilution ecosystem. *eLife*, 9:e57790, 2020.
- [58] M. B. N. Albright, A. B. Chase, and J. B. H. Martiny. Experimental evidence that stochasticity contributes to bacterial composition and functioning in a decomposer community. *mBio*, 10:e00568–19, 2019.
- [59] J. Davies. Inactivation of antibiotics and the dissemination of resistance genes. *Science*, 264(5157):375–382, 1994.
- [60] G. D. Wright. Bacterial resistance to antibiotics: enzymatic degradation and modification. *Adv. Drug Deliv. Rev.*, 57:1451, 2005.
- [61] M. J. Bottery, A. J. Wood, and M. A. Brockhurst. Selective conditions for a multidrug resistance plasmid depend on the sociality of antibiotic resistance. *Antimicrob. Agents Chemother.*, 60(4):2524–2527, 2016.
- [62] D. Hughes and D. I. Andersson. Selection of resistance at lethal and non-lethal antibiotic concentrations. *Curr. Opin. Microbiol.*, 15(5):555–560, 2012.
- [63] D. I. Andersson, S. M. Patin, A. I. Nilsson, and E. Kugelberg. *The Biological Cost of Antibiotic Resistance*, chapter 21, pages 339–348. John Wiley & Sons, Ltd, 2007.
- [64] P. A. P. Moran. *The Statistical Processes of Evolutionary Theory*. Oxford, UK: Clarendon, 1962.
- [65] W. J. Ewens. *Mathematical Population Genetics*. Springer, New York, 2004.
- [66] M. A. van der Horst, J. M. Schuurmans, M. C. Smid, B. B. Koenders, and B. H. ter Kuile. De novo acquisition of resistance to three antibiotics by escherichia coli. *Microb. Drug Resist.*, 17(2):141–147, 2011.
- [67] A. H. Melnyk, A. Wong, and R. Kassen. The fitness costs of antibiotic resistance mutations. *Evol. Appl.*, 8(3):273–283, 2015.
- [68] P. Chesson. Mechanisms of maintenance of species diversity. *Annu. Rev. Ecol. Syst.*, 31:343, 2000.
- [69] R. West and M. Mobilia. Fixation properties of rock-paper-scissors games in fluctuating populations. *J. Theor. Biol.*, 491:110135, 2020.
- [70] I. Bena. Dichotomous markov noise: exact results for out-of-equilibrium systems. *Int. J. Mod. Phys. B*, 20:2825, 2006.
- [71] W. Horsthemke and R. Lefever. *Noise-Induced Transitions*. Springer, Berlin, 2006.
- [72] L. Marrec and A.-F. Bitbol. Resist or perish: fate of a microbial population subjected to a periodic presence of antimicrobial. *PLoS Comput. Biol.*, 16(4):e1007798, 2020.
- [73] T. Tolker-Nielsen and S. Molin. Spatial organization of microbial biofilm communities. *Microb. Ecol.*, 40:75–84, 2000.
- [74] D. Yanni, P. Márquez-Zacarías, P. J. Yunker, and W. C. Ratcliff. Drivers of spatial structure in social microbial communities. *Curr. Biol.*, 29(11):545–550, 2019.
- [75] S. Wright. Evolution in mendelian populations. *Genet.*, 16(2):97, 1931.
- [76] M. Kimura and G. H. Weiss. The stepping stone model of population structure and the decrease of genetic correlation with distance. *Genet.*, 49(4):561, 1964.
- [77] D. T. Gillespie. A general method for numerically simulating the stochastic time evolution of coupled chemical reactions. *J. Comput. Phys.*, 202:403, 1976.
- [78] A. San Millan and R. C. Maclean. Fitness costs of plasmids: a limit to plasmid transmission. *Microbiol. Spectr.*, 5(5):5–5, 2017.

- [79] P. L. Chesson and R. R. Warner. Environmental variability promotes coexistence in lottery competitive systems. *Am. Nat.*, 117(6):923–943, 1981.
- [80] A. Traulsen and C. Hauert. *Stochastic Evolutionary Game Dynamics*, chapter 2, pages 25–61. John Wiley & Sons, Ltd, 2009.
- [81] L. Ridolfi, P. D’Odorico, and F. Laio. *Noise-Induced Phenomena in the Environmental Sciences*. Cambridge University Press, Cambridge, U.K., 2011.
- [82] M. H. A. Davis. Piecewise-deterministic markov processes: a general class of non-diffusion stochastic models. *J. R. Stat. Soc. B*, 46:353–384, 1984.
- [83] W. Horsthemke. Noise induced transitions. In *Non-equilibrium dynamics in chemical systems*, pages 150–160. Springer, 1984.
- [84] C. W. Gardiner. *Handbook of Stochastic Methods*. Springer, USA, 2002.

Parameter	Description	Value
L	side length of square lattice	20
t_{max}	maximum number of microbial generations	500
N_S^0	average number of S cells per deme at $t = 0$	$K(t = 0) - N_{th}$
N_R^0	average number of R cells per deme at $t = 0$	N_{th}
a	reduction in the birth rate of S cells due to drug exposure	0.25
s	resistance metabolic cost for R cells	0.1
m	migration rate	$0-10^{-1}$
K_+	carrying capacity per deme in the mild environment	$10^3-3.2 \cdot 10^4$
K_-	carrying capacity per deme in the harsh environment	80
N_{th}	cooperation threshold	40
ν	environmental switching rate	$10^{-2}-10^0$
δ	environmental switching bias	0.25–0.75

Table 1: **Summary of simulation parameters.** Parameters kept fixed are listed by a single value, other parameters are listed as ranges. The average number of sensitive cells S per deme at $t = 0$ (N_S^0) equals the metapopulation’s carrying capacity at $t = 0$ minus the constant threshold value for cooperation, $K - N_{th}$, which depends on whether the system begins in a harsh or mild environment, $K \in \{K_+, K_-\}$. See Supplementary Fig. S3 for an extended range in ν and δ .

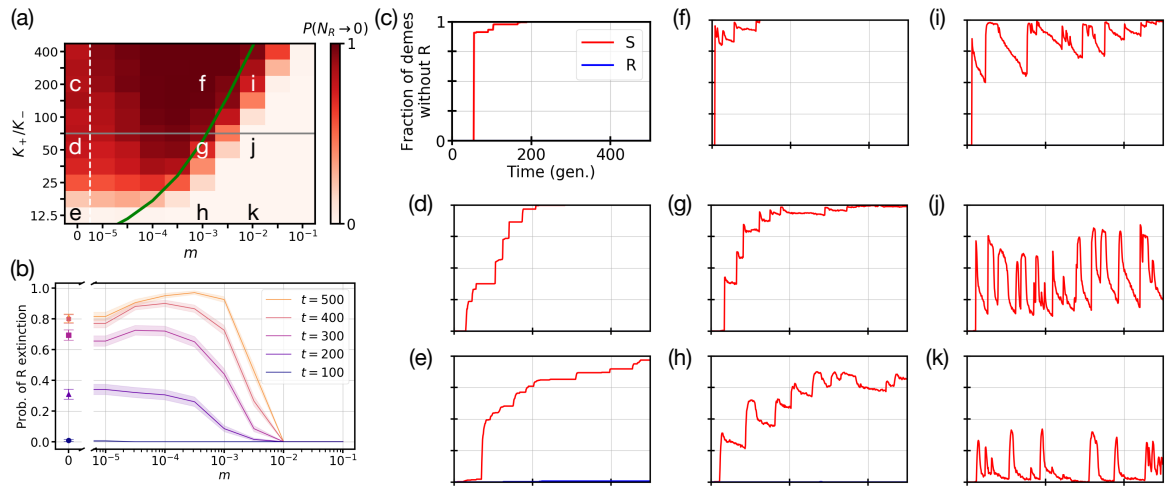


Figure 5: **Revisiting the fluctuation-driven eradication of R cells for intermediate environmental switching with density-dependent migration.** System parameters include an environmental switching rate $\nu = 0.1$, and bias $\delta = 0.5$, with density-dependent migration according to (7). All other parameters ($L, s, a, t_{max}, N_S^0, N_R^0, K_-, N_{th}$) are as listed in Extended Data Table 1 (Methods). **(a)** Same heatmap as in Fig. 4e showing the probability of total extinction of R (resistant) microbes, $P(N_R \rightarrow 0)$, as a function of bottleneck strength, K_+/K_- , and migration rate m after 500 generations; included as an aid to panels (c-k) for clarity. The color bar in panel (a) varies from light to dark red with the darkest red indicating that eradication of R was found in all 200 realisations, $P(N_R \rightarrow 0) = 1$. The white dashed line represents an axis break separating $m = 0$ and $m = 10^{-5}$ on a logarithmic scale. The green line shows the theoretical prediction of Eq. (1). The grey line indicates the bottleneck strength used within panel (b). Annotation letters at specific $(m, K_+/K_-)$ values refer to panels (c-k). **(b)** Same panel as Fig. 4f showing how the probability of R extinction vs migration rate m evolves in time at fixed bottleneck strength, $K_+/K_- = 70.7$. The lines/symbols show the mean across 200 realisations and areas/error bars indicate confidence intervals computed via a Wald interval (Methods). **(c-k)** Temporal evolution of the fraction of R -free demes across the metapopulation for one example realisation in each panel. As indicated in panel (a), migration rates are $m \in \{0, 10^{-3}, 10^{-2}\}$ (left to right) and bottleneck strengths are $K_+/K_- \in \{200, 50, 12.5\}$ (top to bottom). Supplementary Section S3 Movie 4 shows the full spatial metapopulation dynamics for the parameters of panel (i).

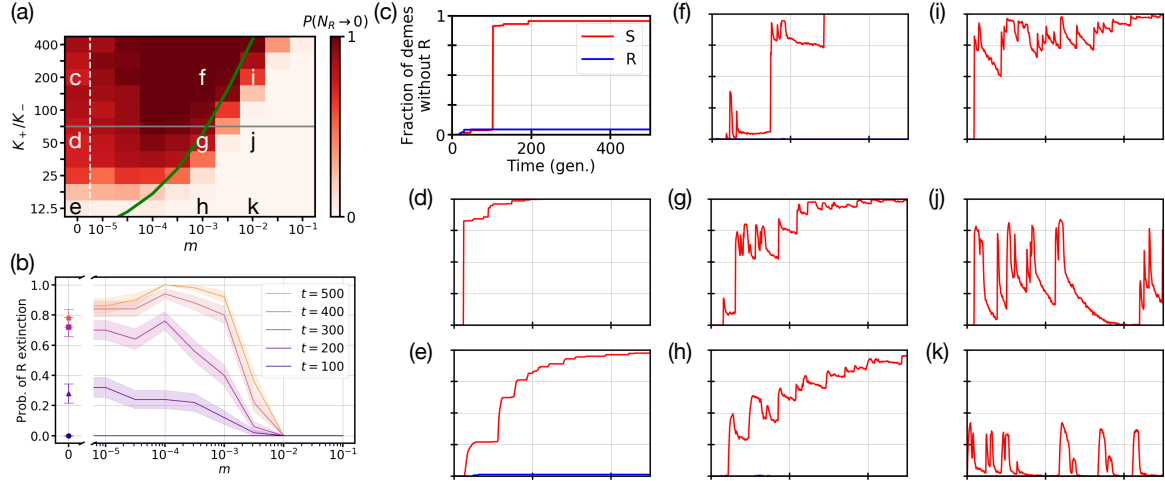


Figure 6: **Exploring the model's robustness: Fluctuation-driven eradication of resistance with density-independent migration.** Same system parameters, $\nu = 0.1$ and $\delta = 0.5$ (see Methods and Extended Data Table 1 for all parameters), and formatting as in Fig. 5, but the migration rate is here taken density-independent according to (8). **(a)** Fraction of realizations resulting in complete eradication of R cells after 500 microbial generations; the heatmap shows the probability of total extinction of R (resistant) microbes, $P(N_R \rightarrow 0)$, depicted by a red colourmap varying from light to dark, with the darkest red indicating eradication of R in all 50 realizations ($P(N_R \rightarrow 0) = 1$). The same panel elements as in Fig. 5 are shown: a white dashed line representing an axis break for the logarithmic scale, a green line theoretical prediction given by (1), a grey line indicating the bottleneck strength used in panel (b), and letters matching panels (c-k) to their respective $(m, K_+/K_-)$ values. **(b)** Probability of R extinction $P(N_R \rightarrow 0)$ as a function of migration rate m for a bottleneck strength of $K_+/K_- = 70.7$ at five different times. The lines/symbols represent the mean across realisations and areas/error bars indicate the confidence intervals computed via the Wald interval (Methods). **(c-k)** Fraction of demes without R cells (red) and without S cells (blue) as a function of time for different values of density-independent migration rate and bottleneck strength: (left to right) $m \in \{0, 10^{-3}, 10^{-2}\}$ and (top to bottom) $K_+/K_- \in \{200, 50, 12.5\}$. Supplementary Section S3 Movie 5 shows the full spatial metapopulation dynamics for the parameters of panel (i).

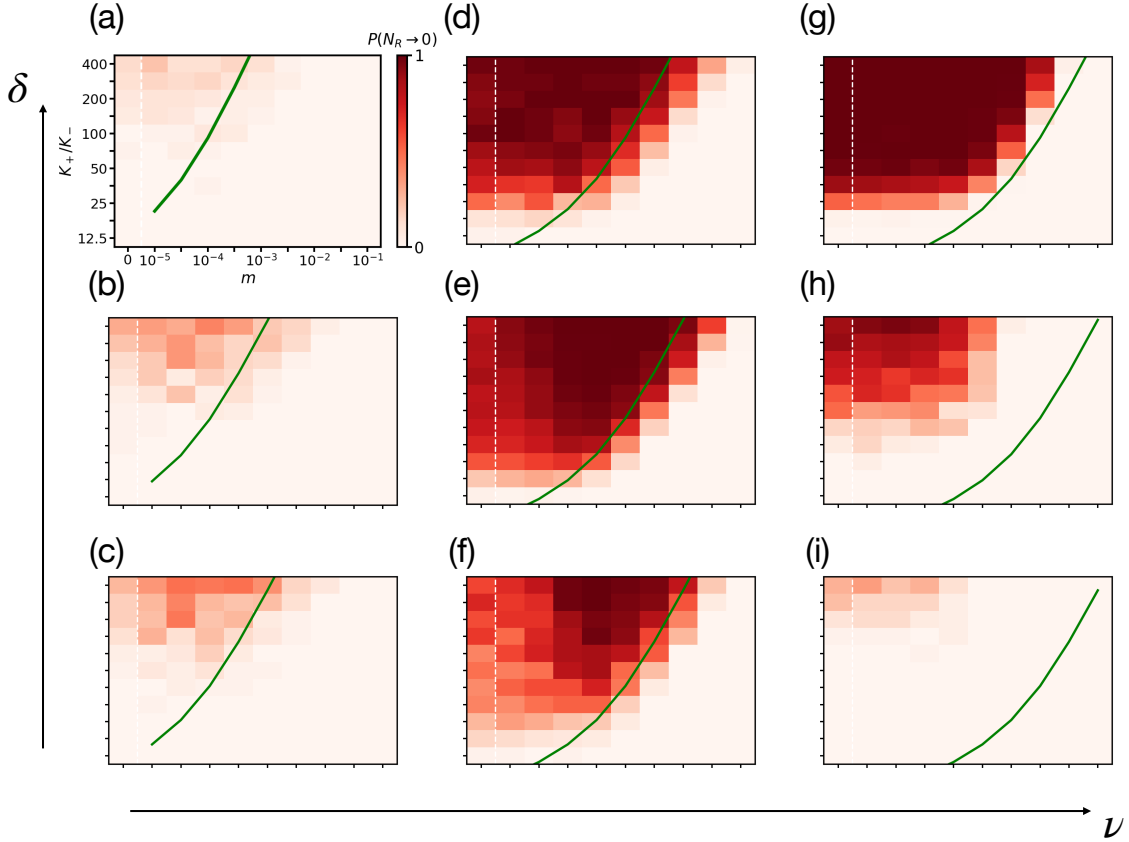


Figure 7: **Exploring the fluctuation-driven eradication of resistance in the (ν, δ) environmental parameter space.** (a-i) Additional heatmaps exploring different environmental switching rates (ν) and biases (δ) showing the probability $P(N_R \rightarrow 0)$ of eradicating R cells as a function of the migration rate m (implemented as in (7)) and bottleneck strength K_+/K_- after 500 microbial generations. The colour bar varies from light ($P(N_R \rightarrow 0) \approx 0$) to dark red ($P(N_R \rightarrow 0) \approx 1$), where the darkest red indicates that all realisations resulted in R eradication across the entire metapopulation, $P(N_R \rightarrow 0) = 1$. The white dashed lines and solid green lines indicate axes breaks on the logarithmic scale and theoretical predictions of Eq. (1), respectively. Panels (e) and (g) correspond to Figs. 4e and 2a, with 200 realisations per pixel, whereas each pixel in the other panels results from 50 independent simulations. The environmental switching rate varies from left to right panels, $\nu \in \{0.01, 0.1, 1\}$, and the environmental bias varies from top to bottom, $\delta \in \{0.75, 0.5, 0.25\}$. Additional heat maps can be found in Supplementary Fig. S3.

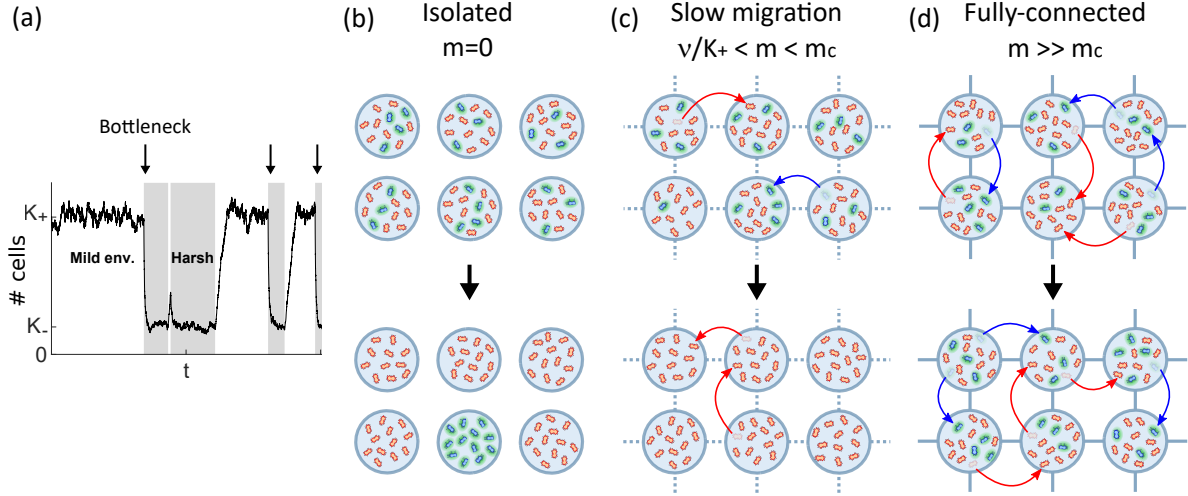


Figure 8: **How slow migration enhances the eradication of resistant cells.** (a) When the metapopulation is subject to an intermediate switching of the environment at a rate $\nu_{\pm} \lesssim 1$, with conditions continuously alternating between mild and harsh, the carrying capacity suddenly varies from $K = K_+$ (mild environment, white background) to $K = K_- \ll 1$ (harsh environment, grey background), bottlenecks appear (arrows), and the spatial fluctuation-driven eradication mechanism of R cells (Figs. 1a bottom and 3a, Methods) sets in. The black trajectory shows an example of the time variation of the total number of cells in a single deme ($N = N_S + N_R$) that is driven by the fluctuating carrying capacity $K(t)$ in the intermediate switching regime. Here, parameters are $\nu_- = 0.125$, $\nu_+ = 0.075$, $K_- = 80$, $K_+ = 400$. Panels (b)-(d) schematically illustrate the state of the metapopulation just before (top row) and after (bottom row) several consecutive bottlenecks at intermediate switching for three different migration scenarios. (b) Prior to any bottleneck, the metapopulation consists of demes containing both R and S cells (top, S cells in red and R cells in blue). After the environmental switches generating a sequence of bottlenecks (black downward arrow, dynamics of $N = N_S + N_R$ as panel (a)), the fluctuation-driven eradication mechanism sets in and can clear resistance from most demes (Methods). However, when $m = 0$ (no migration), there is a chance that R cells take over at least one deme (bottom, blue-only, Supplementary Section S3 Movie 1). Since demes are isolated ($m = 0$), resistant cells may survive locally, since the R -only deme cannot be colonized by S cells. (Following bottlenecks, some demes could still present coexistence of R and S , and more bottlenecks would then be needed to eradicate R , not shown here). (c) Same as in panel (b) with demes connected by slow migration of cells of both types ($\nu/K_+ < m < m_c$; Discussion and Methods). In this scenario, some migration events occur (red/blue arrows indicating migration of S/R cells) and, even if some demes are taken over by R cells, migration allows S cells to recolonise these R -dominated demes (Supplementary Section S3 Movie 2). These become prone to the fluctuation-driven eradication, which can ultimately clear resistance (bottom, all red, $m = 10^{-4} - 10^{-3}$ in Fig. 4, Methods). (d) Same as in (b)-(c) when cells migrate at a high rate ($m \gg m_c$, Eq. (2), Methods), where the metapopulation effectively consists of fully-connected demes. In this scenario, many migration events occur (red and blue arrows), which continuously mix up the composition of the demes, preventing the fluctuation-driven eradication to clear resistance; R and S cells typically coexist in all demes.

Supplementary Information

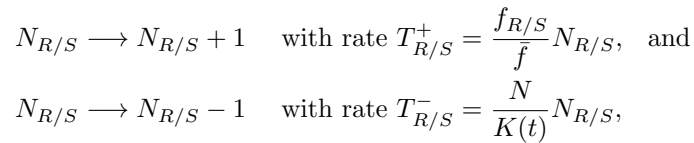
S1 Additional details of the model

In this study, we have considered a spatially structured metapopulation consisting of a square grid of $L \times L$ demes connected by cell migration. Each deme of this explicit spatial model contains microbial co-cultures of two strains of bacteria denoted by R and S . Microbes of strain R are resistant to antimicrobial drugs and can share their protection (cooperative behaviour) with S bacteria that are otherwise sensitive to antibiotic toxins (Main Fig. 1 and Main Methods). A low, homogeneous influx of antimicrobial drug is constantly applied, and the nutrient density (encoded in the carrying capacity K) in the environment can randomly change, alternating sudden periods of feast (mild environment) and famine (harsh environment, Main Fig. 1a). To gain further understanding of the metapopulation model, here we review the main properties of the dynamics of an isolated deme in static and fluctuating environments and discuss the master equation governing the eco-evolutionary dynamics of the metapopulation model.

S1.1 Microbial model in an isolated deme and static environment

As discussed in the main manuscript (Methods), we assume that each resistant cell R generates the resistance enzyme continuously, at a fixed production rate, and that this yields an extra metabolic cost s ($0 < s \ll 1$) which sets the fitness of R to the constant value $f_R = 1 - s$. The growth rate of R is not affected by the presence of antimicrobial drugs in the environment. Moreover, sensitive cells S suffer no resistance-production metabolic cost, but their growth is hindered when exposed to the antimicrobial drug, with a reduction of their fitness from $f_S = 1$ to $f_S = 1 - a$, with $s < a < 1$. In the presence of antimicrobials, the S strain has thus a lower fitness than R .² Sensitive cells recover their intrinsic baseline fitness $f_S = 1$ when there are more resistant cells, N_R , than the *cooperation threshold* N_{th} (Main Methods, Main Fig. 1a), as R cells inactivate enough antimicrobial drug in the same spatial deme to protect S from drug exposure (by setting the drug concentration below its minimum inhibitory concentration) [26, 28, 42, 59, 60].

This can be rationalized by writing the fitness of R and S microbes in a deme as $f_R = 1 - s$ and $f_S = 1 - a \theta[N_{\text{th}} - N_R]$, respectively; where $\theta[z]$ is the Heaviside step function, with $\theta[z] = 1$ if $z > 0$ and $\theta[z] = 0$ if $z \leq 0$. As is customary, and without loss of generality, it is convenient to write the R/S per-capita growth rates in a deme as $f_{R/S}/\bar{f}$, where $\bar{f} = (f_R N_R + f_S N_S)/N$ is the average fitness in that deme [26, 65, 79, 80]. The per-capita death rate of any cell is N/K , where $N = N_R + N_S$ is the total microbial population size in the deme, and K is its carrying capacity, i.e., the average number of microbes that the deme can sustain in a static environment. Therefore, the population dynamics in an isolated deme is given by the birth-death reactions



where $T_{R/S}^\pm$ are the total birth (+) or death (-) rates for the resistant (R) or sensitive (S) strain in the deme under consideration (Main Eq. (4)).

To gain insight into the single-deme microbial dynamics, it is useful to introduce a change of variables: from the number of sensitive N_S and resistant cells N_R to the total population N and the microbial composition $x = N_R/N$, i.e. the fraction of resistant cells. It is convenient to study the dynamics in the deterministic limit under a static environment, with a constant carrying capacity $K_0 \gg 1$. Upon ignoring all stochastic effects, this yields the mean-field rate equations [26, 28]

$$\dot{x} = \frac{f_R - f_S(x, N)}{\bar{f}(x, N)} x(1 - x) \quad \text{and} \quad \dot{N} = N \left(1 - \frac{N}{K_0} \right), \quad (\text{S1})$$

²Note that we consider a biostatic (as opposed to a biocidal) antimicrobial drug. First, we address a low antimicrobial concentration regime, where many drugs present an effectively biostatic action [62, 63, 78]. Second, this non-limiting choice simplifies the mathematical treatment of the model without affecting the qualitative results of this study.

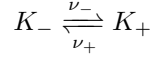
where the dot indicates the time derivative. These ordinary differential equations are decoupled and their stable equilibria are $x \rightarrow N_{\text{th}}/N$ and $N \rightarrow K_0$. The former is reached on a slow evolutionary timescale $\sim 1/s$ since typically $|f_R - f_S| \sim s$, while the latter is attained on a faster ecological timescale ~ 1 [37, 38, 39] (Main Methods). In this mean-field picture, the number of resistant cells tends to the cooperation threshold ($N_R = Nx \rightarrow N_{\text{th}}$) whereas sensitive cells fill the remaining gap to reach the carrying capacity ($N_S \rightarrow K_0 - N_{\text{th}}$) [26]. We emphasize that demographic fluctuations are necessary to reach the absorbing states corresponding to the extinction of one strain ($x = 0$ or $x = 1$). At constant carrying capacity $N \approx K_0$, any strain extinction is typically reached after a long time period, with eventual fixation of R ($x = 1$) if $\frac{N_{\text{th}}}{K_0} \gtrsim \frac{\ln(1-s)}{\ln(1-a)}$, while S fixates the deme otherwise [26].

S1.2 Eco-evolutionary dynamics in an isolated deme subject to a time-fluctuating environment

In this work, we consider a binary environment switching endlessly between mild and harsh conditions (e.g. periods of abundance and scarcity of resources) at a given average rate ν . Each deme is assumed to have the same time-varying carrying capacity $K(t)$ (across the entire metapopulation) expressed in terms of a dichotomous Markov noise (DMN), or telegraph random process, denoted by $\xi(t)$ in the main text:

$$K(t) = \frac{1}{2} [K_+ + K_- + \xi(t)(K_+ - K_-)],$$

(Main Eq. (5)). The dynamics of the total population $N(t)$ in an isolated deme (when $m = 0$) is thus driven by the fluctuating carrying capacity $K(t)$ (Main Methods, Main Extended Data Fig. 8a).³ Thus, $K(t)$ randomly switches between two possible values, $K = K_+ \gg 1$ in the mild environment and $K = K_- < K_+$ in the harsh environmental state, at rates ν_+ and ν_- according to



(Main Methods, Main Eq. (6)). For clarity, we define the mean environmental switching rate $\nu = \frac{\nu_- + \nu_+}{2}$, and the environmental bias $\delta = \frac{\nu_- - \nu_+}{\nu_- + \nu_+}$. The latter characterises the average time spent in each environmental state, and it ranges from $\delta = -1$ (all time spent in K_-) to $\delta = 0$ (symmetric switching, with equal dwelling time in both K_{\pm}), and up to $\delta = 1$ (static environment set at K_+). The expected value of the carrying capacity is thus $\langle K(t) \rangle = \frac{1-\delta}{2} K_- + \frac{1+\delta}{2} K_+$, and its auto-covariance reads $\langle K(t)K(t') \rangle - \langle K(t) \rangle \langle K(t') \rangle = \left(\frac{K_+ - K_-}{2} \right)^2 (1 - \delta^2) e^{-2\nu|t-t'|}$ [70, 71, 81].

If the time-varying carrying capacity is the only source of fluctuations, the dynamics of the total population size in an isolated deme, $N(t)$, is well described by the piecewise deterministic Markov process (PDMP) [82]

$$\dot{N} = \begin{cases} N \left(1 - \frac{N}{K_-} \right) & \text{if } \xi = -1 \\ N \left(1 - \frac{N}{K_+} \right) & \text{if } \xi = 1, \end{cases} \quad (\text{S2})$$

describing the logistic dynamics under the carrying capacity $K = K_{\pm}$ in the environmental state $\xi = \pm 1$, followed by a similar dynamics with $K = K_{\mp}$ after a switch $\xi \rightarrow -\xi$. Upon neglecting demographic fluctuations, the quasi-stationary probability density function for the deme size N can thus be approximated by the stationary PDMP density for fixed $\{\nu, \delta\}$ [26, 27, 28, 37, 38, 39, 71, 81, 83]:

$$\rho(N) = \frac{\mathcal{Z}}{N^2} \left(\frac{K_+ - N}{N} \right)^{\nu(1-\delta)-1} \left(\frac{N - K_-}{N} \right)^{\nu(1+\delta)-1}, \quad (\text{S3})$$

where \mathcal{Z} is a normalisation constant and $N \in [K_-, K_+]$ is a continuous variable.

In environments where switching occurs much more slowly than the ecological timescale ($\nu \ll 1$), N is effectively constant and close to either K_- or K_+ with probability $\frac{1-\delta}{2}$ or $\frac{1+\delta}{2}$, respectively, and the distribution of N as well as $\rho(N)$ are thus bimodal (Supplementary Fig. S1d, Main Methods). For fast-switching environments ($\nu \gg 1$), N is not able to track the frequent changes in $K(t)$, consequently

³It has been shown that both stochastic and periodic fluctuations yield very similar eco-evolutionary dynamics [39]. Hence, our choice of a randomly switching environment is non-limiting, and our results may thus straightforwardly be extended to more general dynamic environments [40].

environmental fluctuations self-average, and N tends to the effectively constant carrying capacity $\mathcal{K} = 1/\langle 1/K(t) \rangle = 2K_-K_+ / [(1+\delta)K_- + (1-\delta)K_+]$, with associated unimodal distributions of N and $\rho(N)$ centred about $N \approx \mathcal{K}$ [26, 37, 38, 39, 40, 69] (Supplementary Fig. S1f, Main Methods). At intermediate switching ($\nu \sim 1$), the distribution of N is complex and cannot be simply explained as resulting from an effective static carrying capacity, or from K being a linear superposition of K_+ and K_- . In this intermediate switching regime, N is thus genuinely subject to time-varying conditions that cannot be represented by an equivalent static environment (Supplementary Fig. S1e).

The above ecological N time evolution in an isolated deme implies that the eco-evolutionary microbial dynamics in slow or fast switching environments can also be effectively mapped to that of a constant environment (Main Methods). The dynamics in a constant environment for a broad range of migration rates $m \in [0, 0.1]$ is discussed in the following Supplementary Section S2. Moreover, the PDMP description of Supplementary Eq. (S2) provides significant insight into the dynamics in the regime of intermediate environmental switching [37, 38, 39] (Supplementary Fig. S1e).

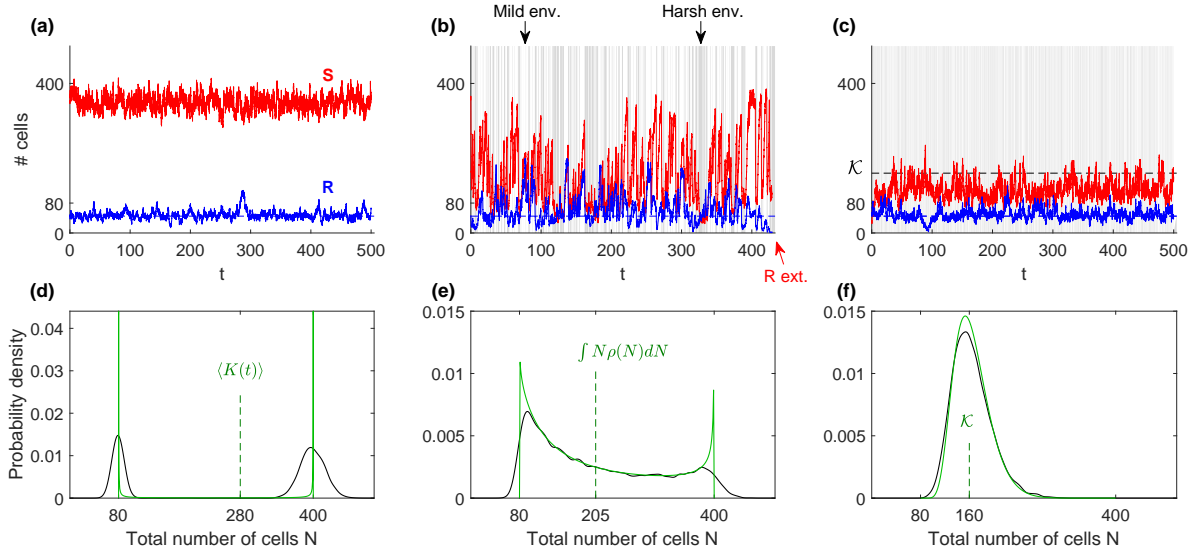
In an isolated deme subject to a slow-switching environment ($\nu \ll 1$), both microbial strains coexist for a typically long time in an effectively constant initial environmental state with a fixed carrying capacity $K_0 = K(t=0) \in \{K_+, K_-\}$ (Supplementary Fig. S1a and Supplementary Section S2). In this setting, R or S cells eventually take over when N_{th}/K_0 is respectively larger or smaller than $\frac{\ln(1-s)}{\ln(1-a)}$ (Supplementary Section S1.1) [26, 28]. In a fast-switching environment ($\nu \gg 1$), we find a similar long-lived coexistence with the effectively constant carrying capacity $K_0 = \mathcal{K}$ and eventual fixation of one strain, see above (Supplementary Fig. S1c, Main Methods). The dynamics in an intermediate switching environment $\nu \sim s$ cannot be reduced to that of a constant environment (Main Methods), and the coupled ecological and evolutionary dynamics may cause the fluctuation-driven eradication of R cells that is extensively discussed in the main manuscript (Supplementary Fig. S1b, Main Methods and Main Discussion).

Laboratory experiments are typically carried out with periodically switching (rather than randomly switching) environments, e.g., [51, 52]. Moreover, natural environmental conditions typically vary continuously in time and magnitude, e.g., [45]. However, we note that the relationship between DMN (telegraph random process), as used in our analysis and other common forms of environmental fluctuations has been extensively studied [39, 40, 70, 83], leading to the conclusion that the DMN is a natural, convenient, and non-limiting choice, in fact therefore close to laboratory experimental conditions.

In isolated demes, the distribution of N is independent of the deme composition [26, 37, 38] (Supplementary Eqs. (S2) and (S3), Supplementary Fig. S1d-f, Main Methods). Its approximation by the PDMP density (S3) is hence expected to hold also in the presence of slow migration $m \ll 1$ at any environmental switching rate ν . We indeed expect slow migration, the most relevant regime for this study (Main Discussion), to have only a minor influence on fluctuations and hence on the distribution of N . We similarly anticipate the above picture and PDMP approximation to hold also for intermediate and fast migration rates. For the latter ($m \gg 1$), all L^2 demes can be viewed as being fully connected (Main Methods).

S1.3 Master equation of the two-dimensional metapopulation model

The full model is a continuous-time multivariate Markov process, and its dynamics with environmental fluctuations and spatial structure is characterised by the probability $P(\{N_R, N_S\}, \xi|t)$ that its microbial population at time t in any given deme, denoted by a two-dimensional position vector \vec{u} , consists of $N_R(\vec{u})$ and $N_S(\vec{u})$ resistant and sensitive cells, in the environmental state $\xi(t) = \pm 1$, with $K(\xi) = K_{\pm}$ when $\xi = \pm 1$. The metapopulation make-up is encoded in $\{N_R, N_S\} \equiv \{N_R(\vec{u}), N_R(\vec{u}'), N_R(\vec{u}''), \dots, N_S(\vec{u}), N_S(\vec{u}'), N_S(\vec{u}''), \dots\}$, where the vectors $\vec{u}, \vec{u}', \vec{u}'', \dots$ denote each of the L^2 demes. Given the migration-mediated interactions between nearest-neighbour demes in the $L \times L$ grid (with periodic boundary conditions; Main Methods), the master equation characterising



Supplementary Figure S1: **Microbial dynamics in an isolated deme under subject to switching environments.** (a) Example stochastic realisation of the number of S (red curve) and R cells (blue solid curve) in an isolated deme vs. time (in microbial generations, Main Methods) for a slow-switching environment (Main Methods), with parameters $N_{th} = 45$ (blue dashed line), $K_+ = 400$, $K_- = 80$, $\nu = 0.001$, $\delta = 0.25$, $s = 0.1$, and $a = 0.25$. In this case, the slow-switching environment starts and stays at the mild environmental state where $K = K_+$ for the whole simulation duration (Supplementary Section S1.2). Sensitive cells thus fluctuate about $N_S \approx K_+ - N_{th}$ while R cells fluctuate about $N_R \approx N_{th}$ (Main Methods). Consequently, the dynamics is the same as in a static environment with carrying capacity $K = K(t = 0)$ (Supplementary Section S1.2, Main Methods). (b) Example stochastic realisation as in panel (a) for an intermediate-switching environment with switching rate $\nu = 0.75 \sim s$ (Main Methods). The environment switches back and forth between harsh ($K = K_-$, grey background shade) and mild conditions (K_+ , white background). The frequent environmental bottlenecks (interfaces from white to grey background) enforce transient dips of N_R until the fluctuation-driven R eradication clears resistance in the deme (red arrow ‘ R ext.’, Main Methods). (c) Same as in panels (a) and (b) for a fast-switching environment with rate $\nu = 10$. The environment switches so often that the microbial dynamics cannot track the changes. The environmental fluctuations thus effectively self average and the carrying capacity can be approximated by the effective constant value \mathcal{K} (i.e. $K \approx \mathcal{K}$; Supplementary Section S1.2, Main Methods). (d) Bimodal quasi-stationary probability density of the total number of individuals $N = N_S + N_R$ in an isolated deme, sampled from 10^4 realisations with the same parameters as in panel (a) (black curve, Main Methods). The solid green line shows the stationary PDMP density $\rho(N)$, given by Supplementary Eq. (S3), as an approximation of the quasi-stationary distribution of N (Supplementary Section S1.2). Simulations were run up to $t = 100$ microbial generations. The dashed vertical green line indicates the average $\langle K(t) \rangle$ which in this regime ($\nu \ll 1$) is close to the mean of the N distribution and to the average of its PDMP approximation $\rho(N)$ (Main Methods). (e) As in panel (d), but with the same parameters as in panel (b). The dashed green vertical line shows $\int_{K_-}^{K_+} N \rho(N) dN$, the average of N with the PDMP density $\rho(N)$ given by Supplementary Eq. (S3), and an approximation of the quasi-stationary average of N as obtained from the simulations. (f) Same as in panels (d) and (e), with the same parameters as in panel (c). The dashed vertical green line indicates $\mathcal{K} = 1/\langle 1/K(t) \rangle$, which in this regime ($\nu \gg 1$) is close to the mean of the probability distribution of N and to the mean of its PDMP approximation $\rho(N)$ (Supplementary Section S1.2, Main Methods).

the stochastic time-evolution of the metapopulation reads [84]:

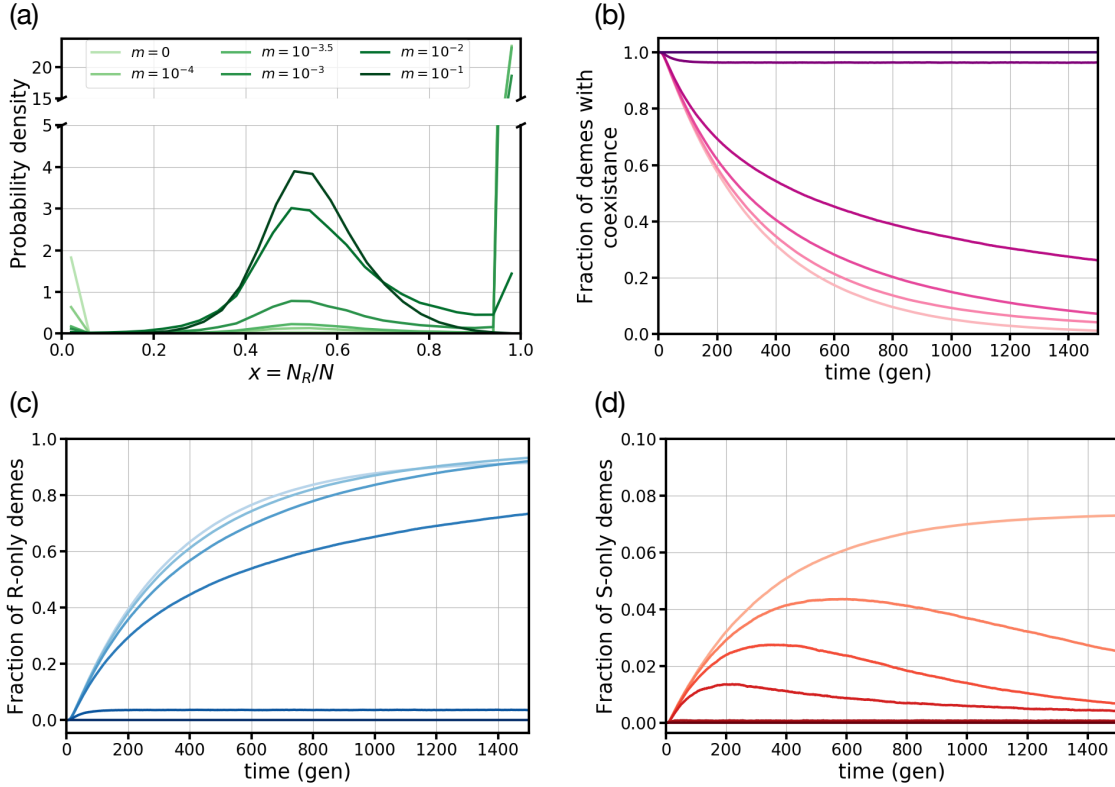
$$\begin{aligned}
\frac{\partial P}{\partial t} = & \sum_{\vec{u}} \left\{ (\mathbb{E}_R^-(\vec{u}) - 1) T_R^+(\vec{u}) P + (\mathbb{E}_R^+(\vec{u}) - 1) T_R^-(\vec{u}) P + (\mathbb{E}_S^-(\vec{u}) - 1) T_S^+(\vec{u}) P + (\mathbb{E}_S^+(\vec{u}) - 1) T_S^-(\vec{u}) P \right. \\
& + \sum_{\vec{u}' \text{ n.n. } \vec{u}} \left[(\mathbb{E}_R^+(\vec{u}') \mathbb{E}_R^-(\vec{u}) - 1) T_R^M(\vec{u}' \rightarrow \vec{u}) P + (\mathbb{E}_R^+(\vec{u}) \mathbb{E}_R^-(\vec{u}') - 1) T_R^M(\vec{u} \rightarrow \vec{u}') P \right. \\
& \left. \left. + (\mathbb{E}_S^+(\vec{u}') \mathbb{E}_S^-(\vec{u}) - 1) T_S^M(\vec{u}' \rightarrow \vec{u}) P + (\mathbb{E}_S^+(\vec{u}) \mathbb{E}_S^-(\vec{u}') - 1) T_S^M(\vec{u} \rightarrow \vec{u}') P \right] \right\} \\
& + \nu_{-\xi} P(\{N_R, N_S\}, -\xi|t) - \nu_{\xi} P(\{N_R, N_S\}, \xi|t), \tag{S4}
\end{aligned}$$

where $\mathbb{E}_{R/S}^{\pm}(\vec{u})$ are shift operators that increase (+) or decrease (−) the number of R or S cells in deme \vec{u} , i.e., they increase or decrease by one the value of $N_R(\vec{u})$ or $N_S(\vec{u})$, which are the components of the set $\{N_R, N_S\}$ that correspond to deme \vec{u} . To simplify the notation, except in the last line, we dropped all explicit dependencies on $\{N_R, N_S\}$, ξ , and t . The birth $T_{R/S}^+(\vec{u})$ and death $T_{R/S}^-(\vec{u})$ rates in a given deme \vec{u} are defined by Main Eq. (4), where the dependence on \vec{u} is dropped for simplicity. The total rate $T_{R/S}^M(\vec{u} \rightarrow \vec{u}')$ for one R or S cell migrating from a deme \vec{u} to a nearest neighbour deme \vec{u}' corresponds to $\frac{m}{4} \frac{N(\vec{u})}{K(t)} N_{R/S}(\vec{u})$, defined by the rate of Main Eq. (7) with the last factor $N(\vec{u})$ replaced by $N_{R/S}(\vec{u})$. Similarly, the total migration rate for the alternative form given by Main Eq. (8) is $T_{R/S}^M(\vec{u} \rightarrow \vec{u}') = \frac{m}{4} N_{R/S}(\vec{u})$. In the master equation, the sum $\sum_{\vec{u}}$ runs over all L^2 demes in the metapopulation; the sum $\sum_{\vec{u}} \sum_{\vec{u}' \text{ n.n. } \vec{u}}$ extends over the four nearest neighbours (n.n.) \vec{u}' of each deme \vec{u} ; in the last line we adopt the notation $\nu_{\xi} \equiv \nu_{\pm}$ when $\xi = \pm 1$. The right-hand side of the first line encodes births and deaths of resistant and sensitive cells for each deme \vec{u} ; the second and third lines describe the inward and outward migration of resistant or sensitive microbes, respectively; and the final line accounts for the random environmental switching. This multivariate master equation can be simulated using the stochastic methods described in the Main Computational Methods section. Note that demographic fluctuations eventually lead to the extinction of the entire metapopulation, but this phenomenon is unobservable as it typically occurs after an enormous time that grows dramatically with the system size.

S2 Resistant and sensitive cells coexist in static environments

In this section we assess how spatial migration influences the survival of R and S cells in static environments, where the carrying capacity K is constant. Importantly, we demonstrate that the parameters yielding efficient eradication of R in intermediate switching environments (Main Figs. 2-4 and Main Extended Data Figs. 5-8) lead here to long-lived coexistence of both types of cells, with R gradually dominating (Supplementary Fig. S2; see also Supplementary Section S1.1). We first focus on the case of independent demes ($m = 0$). We then show that fast migration enhances coexistence. Next, we find that slow but nonzero migration promotes the dominance of R , which is the opposite of what happens under intermediate switching environments where in contrast S cells dominate over R (Main Discussion). We also discuss how these results specific to static environments extend to both very slow ($\nu \ll 1$) or very fast ($\nu \gg 1$) switching environments.

When a spatial environment is composed of fully segregated demes, without migration connecting them ($m = 0$), these evolve independently of each other. In the case of static environments, as discussed in Supplementary Section S1.1 (and in Main Methods), the dynamics in each deme tends to a long-lived coexistence equilibrium that is situated at the edge of microbial cooperation ($N_R = N_{\text{th}}$ and $N_S = K - N_{\text{th}}$) (in Supplementary Fig. S2, R cells tend to dominate because $\frac{N_{\text{th}}}{K_0} > \frac{\ln(1-s)}{\ln(1-a)}$ [26], see end of Supplementary Section S1.1). Hence, in the absence of migration ($m = 0$), we find very long-lived strain coexistence at the metapopulation level, with a slow increase in the number of R -only (and few S -only) demes (lightest curve $m = 0$ in Supplementary Figs. S2b-d). The fraction of resistant cells ($x \equiv N_R/N$) thus follows a bimodal distribution for $m = 0$: A dominant peak at $x = 1$ as R cells take over most of the isolated demes, and a secondary peak at $x = 0$ for the sites where S takes over by chance (darkest curve $m = 0$ in Supplementary Fig. S2a).



Supplementary Figure S2: **Migration shapes the coexistence of S and R cells in constant environments.** (a) Probability density of the microbial composition x (i.e., the fraction of R cells) in a deme after $t = 1500$ microbial generations computed in bins of width $\Delta x = 0.04$. Migration rates are $m \in \{0, 10^{-4}, 10^{-3.5}, 10^{-3}, 10^{-2}, 10^{-1}\}$ (light to dark colour, bottom to top curves); with constant carrying capacity $K = 80$, resistance cooperation threshold $N_{\text{th}} = 40$, resistance metabolic cost $s = 0.1$, drug impact on sensitive growth $a = 0.25$, on a square grid of $L \times L = 100 \times 100$ demes; data were averaged over 50 realizations, and error bars are smaller than the line thickness. (b) Fraction of sites in the metapopulation with coexisting R and S cells as a function of time for the same parameters as in panel a. Migration rates increase from bottom to top curves. (c) Same as in panel b for the fraction of R -only demes in the entire metapopulation; migration rates increase from top to bottom curves. (d) Same as in panel c for the fraction of single-strain S demes.

As cell migration increases, the demes interconnect ($m > 0$). Thus, the extinction of one strain in a given deme is no longer an irreversible process, since microbes of the extinct strain can recolonise each deme by migrating from neighbouring sites ('asterisk' and 'cross' demes connected by blue arrow in Main Fig. 1b, Main Methods). Therefore, migration in static environments generally enforces and enhances coexistence. Indeed, as shown in Supplementary Fig. S2b, faster migration always promotes a larger number of multi-strain demes. At sufficiently high migration rates, the frequent mixing of microbes between demes avoids local strain extinction (no decay in the fraction of strain-coexisting demes for $m \geq 10^{-2}$ in Supplementary Fig. S2b), and the composition of each deme then fluctuates about the coexistence equilibrium (x accumulates about $x_{\text{th}} = 0.5$ in Supplementary Fig. S2a). In the fast migration limit $m \gg 1$, demes are fully connected, and the distribution in the fraction of R cells accumulates narrowly about the previous coexistence equilibrium (not shown). After an unobservably long time, assuming $K \gg 1$, the metapopulation will most likely become a homogeneous monoculture of R cells as these typically fixate faster than S cells (Supplementary Fig. S2c-d).⁴

Critically, slow but nonzero migration here enhances the fixation probability of R cells, as opposed to enhancing R eradication as found in environments switching in the intermediate regime (Main

⁴Note that the final state is the full extinction of the metapopulation, but this will occur after an even much longer time.

Discussion and Extended Data Fig. 8c). In a static environment, we thus find the largest fraction of R -only demes at slow yet, perhaps counterintuitively, nonzero migration, where the fraction of S -only demes is already low: In Supplementary Fig. S2c the graphs $m = 10^{-4}$ and $10^{-3.5}$ overtake the $m = 0$ curve at $t \approx 1100$ and $t \approx 1400$, respectively; the curves for $m = 10^{-4}$ and $m = 10^{-3.5}$ in fact decay faster than any others in S2d, and feature the highest fraction of R -only demes and lowest fraction of S -only demes in S2a. Although quantitatively small, these changes unveil a qualitatively relevant phenomenon: Namely, in this slow-switching regime, migration is strong enough to foster R recolonisation, but also sufficiently weak to prevent S recolonisation. When the metapopulation is subject to a time-fluctuating environment that varies at an intermediate switching rate, and there is slow cell migration, we have exhaustively discussed in the main manuscript that a similar phenomenon of much stronger effect enhances the eradication of resistance (Main Discussion). In time-switching environments, we have indeed in remarkable contrast seen that S cells dominate and slow migration enhances and speeds up the fluctuation-driven eradication of R cells (Supplementary Section S3 Movie 2).

All the above results for static environments can be extended to time-fluctuating environments when the switching rate is very low (e.g. very long periods of feast and famine), ($\nu \ll 1$), and under fast switching, ($\nu \gg 1$). The rationale is that in extremely slow/fast-varying environments the ecological and evolutionary dynamics are essentially independent, and can be effectively reduced to those arising in equivalent static environments (Supplementary Fig. S1, end of Supplementary Section S1.2, Main Methods).

S3 Supplementary simulation movies

In this section we caption and describe the movies uploaded in the Open Science Foundation repository, and electronically available at <https://doi.org/10.17605/OSF.IO/EPB28>.

Movie 1: Resistant cells can survive in switching environments when demes are fully isolated. Example of spatial microbial dynamics for a single realisation of a metapopulation without migration ($m = 0$) subject to a slow-intermediate switching environment (Main Methods). The simulation parameters are $L = 20$, $\nu = 0.001$, $\delta = 0$, $K_- = 80$, $K_+ = 1414$, $N_{\text{th}} = 40$, $s = 0.1$ and $a = 0.25$; all the other parameters are as listed in Main Extended Data Table 1. The simulation was run for 500 Monte Carlo Steps (i.e., microbial generations; Main Methods). **Left:** microbial composition of the 20×20 square grid of demes evolving in time. Red pixels indicate demes with S cells only, blue pixels depict R -only demes, and pink pixels are demes where both R and S cells coexist. **Top right:** temporal evolution of the average number of S (red trace) and R cells (blue) over all multi-strain demes (pink demes in left panel) where both strains coexist (similar to Main Fig. 3c). **Bottom right:** temporal evolution of the fraction of single-strain demes where only S (red traces) or R cells (blue) survive (similar to Main Fig. 3d). Since demes are fully isolated (no microbial migration $m = 0$), the extinction of R or S cells is irreversible in each deme (when a pink pixel in left panel becomes red or blue, it remains so as no recolonisation is possible; blue and red traces in the bottom right panel do not decrease in time). In persistent harsh conditions (low total number of cells, top right panel), R can by chance take over some demes due to demographic fluctuations, while S only takes over a few demes (several blue pixels and a few red pixels replace pink pixels in left panel, blue trace increases faster than red trace in bottom right panel, Supplementary Section S1.1, Main Methods). In a mild environment (high total number of cells, mostly S , top right panel), S can still take over a few demes, but R typically cannot (a few additional red pixels replace pink ones in left panel, the red trace still increases while the blue stays constant in the bottom right panel, Supplementary Section S1.1, Main Methods). When the metapopulation experiences each environmental switch from mild to harsh conditions (occurrence of a bottleneck), the fluctuation-driven eradication mechanism wipes out resistance in many coexisting demes (many pink pixels become red in left panel, dip in the red and blue traces in top right panel, big red spike in the red trace of bottom right panel, Main Methods). After a sufficiently long time, following a sequence of bottlenecks, the metapopulation will be composed of many S -only demes (red pixels in left panel) and fewer, spatially scattered R -only demes (blue pixels), without any demes where both strains coexist (no pink pixels). For these set of parameters, resistance thus survives in the metapopulation.

Movie 2: Slow migration can enhance the fluctuation-driven eradication mechanism. Legend as in Supplementary Movie 1 but with slow cell migration at rate $m = 0.001$, implemented according to Main Eq. (7). Local strain extinction is now reversible as R and S can recolonise any deme through cellular migration (blue and red pixels can become pink again in left panel, traces can decrease in time in the bottom right panel; Main Methods). Recolonisation events are greatly enhanced when the environment switches to the mild state $K = K_+$ since the number of migration attempts increases with the total population size (higher total number of cells, mostly S , in top right panel, almost all the pixels become pink in the left panel; both traces almost reach zero again in the bottom right panel, Main Methods). As in Supplementary Movie 1, population bottlenecks lead to fluctuation-eradication of resistance in many coexisting demes (many pink pixels suddenly become red in left panel, dip in red and blue traces in top right panel, red spike in bottom right panel, Main Methods). This process continues cyclically until R cells are eradicated across the whole metapopulation, an outcome that is impossible to achieve for these parameters in the absence of migration (Main Discussion, Main Methods). Note that full R eradication is not shown in this Movie as it occurs shortly after $t = 500$.

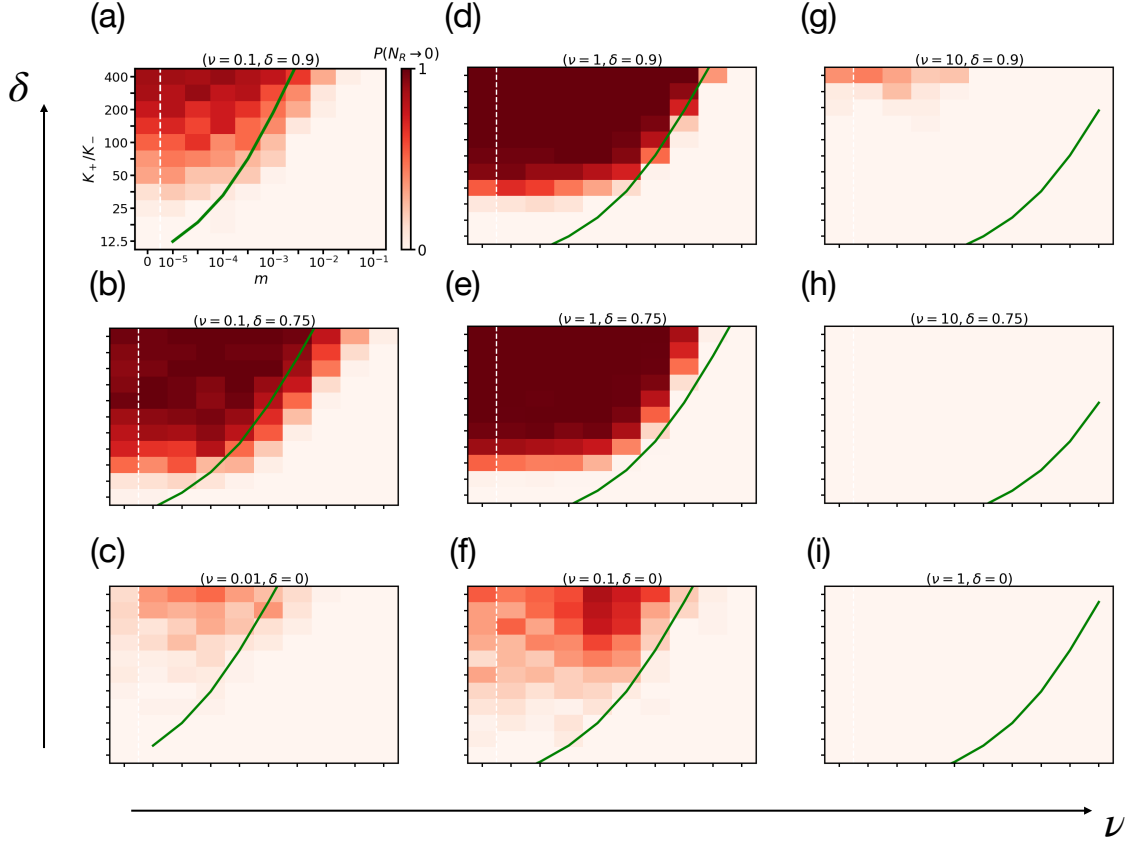
Movie 3: Fluctuation-driven eradication of R . Legend as in Supplementary Movies 1 and 2 but with average environmental switching rate $\nu = 0.1$, bias $\delta = 0.5$, high carrying capacity $K_+ = 2000$, and migration rate $m = 0.001$. This movie corresponds to the same realisation that is shown in Main Fig. 3. In this case, the slow but nonzero migration rate m and the shorter time spent in the harsh environment than in the mild one ($\delta > 0$) prevents R cells to take over any demes (no blue pixels in left panel and zero blue curve in bottom right panel at all times). The intermediate environmental switching causes many successive bottlenecks that eradicate R in an increasing number of demes, hence overcoming cellular mixing driven by migration (accumulation of burst of red pixels in left panel, accumulation of spikes in the red trace of the bottom right panel; Main Discussion and Methods). Ultimately, after $t = 500$ microbial generations, the R strain is almost entirely wiped out from the metapopulation, and will be fully cleared after a few more generations (all but two pixels are red in left panel, red trace almost reaches 1 at $t = 500$ in the bottom right panel).

Movie 4: Fluctuation-driven eradication mechanism with density-dependent migration. Legend as in Supplementary Movie 3 but with high carrying capacity $K_+ = 16000$ and migration rate $m = 0.01$. As in Movies 1-3, the density-dependent migration is implemented according to Main Eq. (7). This movie corresponds to the realisation shown in Main Extended Data Fig. 5i. In this case, the observed behaviour is similar to that of Movie 3: R cannot take over any deme (no blue pixels in left panel and zero blue curve in bottom right panel) and the fluctuation-driven eradication almost eliminates resistance after 500 generations (very few pink pixels left in left panel, red trace almost reaches 1 in the bottom right panel).

Movie 5: Fluctuation-driven eradication mechanism with density-independent migration. Legend and parameters as in Movie 4, but here migration is density-independent according to Main Eq. (8). This case corresponds to the realisation shown in Main Extended Data Fig. 6i. A direct comparison with Movie 4 reveals qualitatively similar results in all panels.

S4 Further exploration of fluctuation-driven eradication of resistance for different (ν, δ)

See Supplementary Fig. S3.



Supplementary Figure S3: **Further exploration of fluctuation-driven eradication of resistance in the (ν, δ) parameter space.** Same as in the main Figure 7, we show the heatmaps of the probability of R extinction, $P(N_R \rightarrow 0)$, as a function of K_+/K_- and m for additional values of $(\nu, \delta) = (0.1, 0.9)$ (a), $(0.1, 0.75)$ (b), $(0.01, 0.0)$ (c), $(1, 0.9)$ (d), $(1, 0.75)$ (e), $(0.1, 0)$ (f). All the other parameters are as in the Extended Data Table 1 of the main text. Dark red corresponds to $P(N_R \rightarrow 0) \approx 1$ and light to $P(N_R \rightarrow 0) \approx 0$.